

Advanced Functional Materials

Colossal reversible barocaloric effects in layered hybrid perovskite (C₁₀H₂₁NH₃)₂MnCl₄ under low pressure near room temperature.

--Manuscript Draft--

Manuscript Number:	adfm.202105154R1
Article Type:	Research Article
Corresponding Author:	Pol Lloveras Universitat Politècnica de Catalunya Sant Adrià del Besòs, Barcelona (Catalunya) SPAIN
Corresponding Author E-Mail:	pol.lloveras@upc.edu
Order of Authors:	Junning Li, PhD Student María Barrio, Associate Professor David J. Dunstan, Full Professor Richard Dixey Xiaojie Lou, Full Professor Josep-Lluís Tamarit, Full Professor Anthony E. Phillips Pol Lloveras
Keywords:	Barocaloric effects; hybrid layered perovskites; Calorimetry; phase diagram; Raman scattering
Manuscript Classifications:	ENGINEERING - mechanical/structural properties, fabrication/manufacturing/processing, 3D printing, composites, actuators, robotics, thermal properties
Section/Category:	
Abstract:	We report barocaloric effects in a layered hybrid organic-inorganic compound, (C ₁₀ H ₂₁ NH ₃) ₂ MnCl ₄ , that are reversible and colossal under pressure changes below 0.1 GPa. This barocaloric performance originates in a phase transition characterized by different features: A strong disordering of the organic chains, a very large volume change, a very large sensitive of the transition temperature to pressure and a small hysteresis. Our obtained values are unprecedented among solid-state cooling materials at such low pressure changes and demonstrate that colossal effects can be obtained in compounds other than plastic crystals. The temperature-pressure phase diagram displays a triple point indicating enantiotropy at high pressure.
Author Comments:	Dear Editor, I would very much appreciate if the author Junning Li could also appear as corresponding author (along with me) if the manuscript is finally accepted for publication. Thank you very much for your consideration. Sincerely yours, Pol Lloveras
Additional Information:	
Question	Response
Please submit a plain text version of your cover letter here.	Dear Editor, We hereby submit a revised version of the manuscript entitled "Colossal reversible barocaloric effects in layered hybrid perovskite (C ₁₀ H ₂₁ NH ₃) ₂ MnCl ₄ under low

	<p>pressure near room temperature". We really appreciate the time and effort the Reviewers have devoted to our manuscript and thank their comments very much, which have helped to improve it. We are also very pleased to see that both give a positive assessment of our work and consider it worthy for publication after minor changes. In this resubmission we provide a point-by-point response to the Reviewers' comments with the manuscript with changes highlighted. We hope that our revised manuscript will now be considered suitable for publication in Advanced Functional Materials.</p> <p>Sincerely yours,</p> <p>On behalf of all co-authors</p> <p>Dr. Pol Lloveras</p>
<p>Does the research described in this manuscript include animal experiments?</p>	<p>No</p>
<p>Does the research described in this manuscript include human research participants (including for experiments with sensors or wearable technologies) or tissue samples from human subjects (including blood or sweat)?</p>	<p>No</p>
<p>Do you or any of your co-authors have a conflict of interest to declare?</p>	<p>No. The authors declare no conflict of interest.</p>
<p>This journal's Expects Data Policy requires a Data Availability Statement (even if no data are shared), which will be published alongside your manuscript if it is accepted for publication.</p> <p>Do you choose to share the research data described in this manuscript?</p>	<p>Yes</p>
<p>Please choose the appropriate template for your Data Availability Statement from this list, copy it into the textbox below, and insert the URL/DOI link, repository name, etc., where applicable.</p> <p>When data are available and linked, please include a citation of the data in the reference list of your manuscript.</p> <p>as follow-up to "This journal's Expects Data Policy requires a Data Availability Statement (even if no data are shared),</p>	<p>The data that support the findings of this study are available from the corresponding author upon reasonable request.</p>

<p>which will be published alongside your manuscript if it is accepted for publication.</p> <p>Do you choose to share the research data described in this manuscript?"</p>	
<p>Response to Reviewers:</p>	<p>POINT-BY-POINT RESPONSE TO REVIEWERS</p> <p>REVIEWER #1</p> <p>Reviewer's Comment:</p> <p>It is impressive that the compound (C₁₀H₂₁NH₃)₂MnCl₄ performs better BC effects when compared with other BC materials. Therefore, this study presents a good example for developing colossal barocaloric materials. Overall, I suggest that this work can be potentially as a good contribution to Advanced Functional Materials upon further revision.</p> <p>Response: We thank the Reviewer for his/her positive assessment of our work.</p> <p>*****</p> <p>Reviewer's Comment:</p> <p>1. Authors should demonstrate the detailed processes of obtaining the structural information for the compound (C₁₀H₂₁NH₃)₂MnCl₄, rather than just citing references.</p> <p>Response: In the revised version of the manuscript, Rietveld refinement has now been performed to determine the high- and low-temperature structures. The corresponding CIFs have been uploaded to CCDC as usual (CCDC numbers 2096682 and 2096683) and the details have been included in the Supplementary Material.</p> <p>*****</p> <p>Reviewer's Comment:</p> <p>2. What is the yield of the chemical reaction? Please provide the synthetic yield of the compound (C₁₀H₂₁NH₃)₂MnCl₄.</p> <p>Response: We prepared our target sample through the following reaction:</p> $2(\text{C}_{10}\text{H}_{21}\text{NH}_2) + 2\text{HCl} + \text{MnCl}_2 \rightarrow (\text{C}_{10}\text{H}_{21}\text{NH}_3)_2\text{MnCl}_4$ <p>The synthetic yield of the reaction is 90%. However, the as-prepared power sample needs to be washed and recrystallized from ethanol. The yield of the recrystallizing step is 80%, which depends on the (controllable) cooling speed. Thus, considering the multi-step reaction, the total yield of the compound is total yield (%) $\approx (0.9 \cdot 0.8) \cdot 100 \approx 72\%$. This value has now been included into the Experimental Section.</p> <p>*****</p> <p>Reviewer's Comment:</p> <p>3. In Figure S3, the unit cell volume would expand gradually when the temperature increases under the first situation (blue dots), which may be related to the thermal expansion. However, under the second situation (red dots), the volume shows shrinkage as the temperature increases, which is hard to understand and learn. Please</p>

give some explanations.

Response: As mentioned in our response to Reviewer's Comment #1, in the revised version of the manuscript, Rietveld refinement has now been performed to determine the high- and low-temperature structures, whose details have been included in the Supplementary Material. From the obtained structures, pattern matching of the temperature-dependence patterns has been performed to determine the temperature-dependence of the lattice parameters (Figure S4 of the Supplementary Material). While for the low-temperature phase the same results have been obtained as compared to those previously calculated, for the high-temperature phase the resulting dependence of volume on temperature shows a smooth increase with a small thermal expansion coefficient $\alpha_V = 7 \cdot 10^{-5} \text{ K}^{-1}$. Importantly, this is fully consistent within error with the entropy curves calculated previously because the latter are calculated using $(\partial V/\partial T)_p$ in the low-temperature phase and because in the high-temperature phase the small and positive value for $(\partial V/\partial T)_p$ yields isothermal entropy changes outside the transition that are very small as compared to the changes occurring at the transition, and negative in sign upon a pressure increase (see Figure 4a,b in the manuscript).

On the other hand, lattice parameter *b* is observed to undergo a shrinkage upon increasing temperature. While the study of this behavior is beyond the scope of this work, it is worth mentioning that this feature has been observed in other layered perovskites (Huang et al., Phys. Rev. Lett. 2016, 117 115901) as well as in non-layered perovskites (Shang et al., Chem. Eur. J. 2014, 20 1146).

Notice also that the number of formula units per unit cell $Z = 4$ was used by mistake, which has now been corrected ($Z = 2$) (panel (e) of Figure S4).

Reviewer's Comment:

4. How about the thermal stability of the compound $(\text{C}_{10}\text{H}_{21}\text{NH}_3)_2\text{MnCl}_4$? Please illustrate.

Response: The compound has shown to be thermally stable along several years after synthesization, being stored without any particular condition. On the other hand, we have also observed that the thermodynamic transition properties are not modified after thermal cycling across the phase transition at different pressures applied randomly. In this sense, our observations are fully consistent with the findings in C. R. Raj et al., "Manganese-based layered perovskite solid–solid phase change material: Synthesis, characterization and thermal stability study", Mech. Mater. 2019 135 88-97, where the thermal stability of $(\text{C}_{10}\text{H}_{21}\text{NH}_3)_2\text{MnCl}_4$ was specifically investigated.

Reviewer's Comment:

5. To better observe the temperature-dependent spectral changes, authors should point out and mark the characteristic peaks or bands in the Raman spectra (Figure 2a-d).

Response: Following the Reviewer advice, we have included dashed lines indicating the characteristic peaks and explanatory key words in Figures 2a-d.

Reviewer's Comment:

6. The classical perovskite usually has the structures of ABO_3 or A_2BO_6 , so if the hybrid in this work is labeled as perovskite, authors need to discuss more about the perovskite structures.

Response: The structure of the hybrid studied in this work does not exhibit the true

perovskite structure ABO₃, which consists of a 3D corner-sharing octahedra. Instead, compounds such as those with general formula (R-NH₃)₂BX₄ [R-NH₃⁺ = interlayer alkylammonium chain cations, B = divalent metal and X₄⁻ = halide anions], are called layered perovskites because they exhibit a perovskite-like structure projected on a reduced dimensionality, consisting of corner-sharing BX₆ octahedra in 2 dimensions that form inorganic sheets in the (ab) planes. In this case, the length of the interlayer organic chain prevents the 3D corner-sharing along the c axis between octahedra belonging to different layers, as it does occur in true perovskites. Clear descriptions of the 2D perovskite structures and their relation to 3D true perovskites can be found in the following references:

- Cauê F. Ferreira, PhD Thesis, Controlling the thermodynamic phase stability of hybrid perovskites with organic media, University of Florida (2016)

- L. Mao, C. C. Stoumpos, M. G. Kanatzidis, Two-Dimensional Hybrid Halide Perovskites: Principles and Promises, J. Am. Chem. Soc. 2019, 141, 1171–1190.

- D. B. Mitzi, Templating and structural engineering in organic–inorganic perovskites, J. Chem. Soc., Dalton Trans., 2001, 1–12.

To make this point clearer in the revised version of the manuscript, we have modified the text and included the two last references above.

Reviewer's Comment:

7. Following comment 6, in my view, hybrid perovskites and metal organic halides are hot topics in materials science, to arouse a broad interest from readership in this field, several strongly related works on hybrid perovskites materials (Angew. Chem. Int. Ed. 2019, 58, 15128; Chem. Soc. Rev., 2021, 50, 5564) and structural and property modulation of metal organic halides (Adv. Mater. 2021, 33, 2007571; Nat. Commun. 2020, 11, 4649) can be enriched as references.

Response: Following the Reviewer's advice, we have included the first two references in the Introduction's section. We prefer to leave out the other two as they are particular cases not directly linked with our work.

Reviewer's Comment:

8. The language of this manuscript could be further polished.

Response: Following the Reviewer's comment, the text has been improved.

REVIEWER #2

Reviewer's Comment:

This work is a nice advance in the field of barocalorics materials. The characterizations are comprehensive and the results are convincing. Therefore, I have no doubt to recommend its publication in Advanced Functional Materials provided that the authors can address the following a few minor points:

Response: We really appreciate the Reviewer for his/her very positive assessment of our work.

Reviewer's Comment:

1. The high- and low-temperature structures of (C₁₀H₂₁NH₃)₂MnCl₄ should be provided to facilitate the readers' understanding.

Response: Following the Reviewer suggestion, in the revised version of the manuscript the diffraction patterns of the low-temperature phase at 295 K and of the high-temperature phase at 330 K were refined by means of a Rietveld refinement procedure (Rietveld, J. Appl. Crystallogr. 1969, 2 65-71), using TOPAS-Academic v.7 (A. A. Coelho J. Appl. Cryst. 2018, 51 210). Because of this task, Richard Dixey and Anthony E. Phillips have been included in the author list.

In the low-temperature phase, we refined a model based on the reported structure in space group P2₁/a. The decylammonium ion was modelled as a rigid body in which all C-C bond lengths and C-C-C bond angles were fixed, while the C-C-C-C torsion angles refined freely. H atoms were placed by geometry. The positions of the Cl atoms were restrained so that the Mn-Cl bond lengths had approximately their reported values of 2.485 and 2.584 Å and the Cl-Mn-Cl angles were approximately 90°. The Mn atom sits on the center of symmetry at the origin and has no translational degrees of freedom. Isotropic atomic displacement parameters (ADPs) were refined for all atoms, with the Cl atoms and, separately, the C and N atoms constrained to have the same value. A spherical harmonic correction for preferred orientation was used, refining terms up to eighth order. This gave good agreement with the experimental data (see Figure S1b in the revised Supplementary Material).

To our knowledge, no structural model of the high-temperature phase has previously been reported. Since the transition is first-order, the space group of this phase is not required to be a supergroup of that of the low-temperature phase. However, for simplicity, and by analogy with the related Cd-containing material (R. Kind et al., J. Chem. Phys. 1979, 71 2118), we began by considering possible space groups among the minimal supergroups of P2₁/a. These can be divided into two categories: the translationengleiche supergroups, which have orthorhombic symmetry; and the klassengleiche supergroups, which have a new translational symmetry element.

Considering the first possibility, we searched for a possible orthorhombic cell, using simulated annealing to refine the cell parameters in a Pawley fit. It quickly became clear that the experimental pattern could not be reproduced by an orthorhombic cell with the same volume, ruling out the possibility of describing it in a translationengleiche supergroup. On the other hand, a monoclinic cell described it well.

Turning to the second possibility, the obvious potential new translational symmetry element is along the vector (1/2, 1/2, 0), connecting the two Mn atoms. This is easily described by a C-centered cell. There are now only two possible space groups, C2/m and C2/c. By inspection, of these only C2/m is compatible with the observed structure (with cell vectors remaining the same as P2₁/a).

As a final alternative, we also considered a non-supergroup structure in Pbc_a, in which the unit cell doubles along the c axis. This structure occurs in the Pb analogue of this material (A. Lemmerer, D. G. Billing, Dalton Trans. 2012, 41 1146). Considering only the peak positions in a Pawley fit showed that this is indeed a plausible unit cell. However, in Rietveld refinement the structural model gave very poor agreement with the data. We did not, therefore, pursue it further.

We concluded therefore that the best description of these data is given by a C2/m model. In this space group, the Mn and one Cl atom must sit on special positions, and have no translational degrees of freedom in Rietveld refinement. The other Cl atom and the decylammonium ion sit on, or are disordered about, the mirror plane. QENS measurements (F. Guillaume et al., Mol. Phys. 1989, 67 665) suggest that the dominant conformation in the HT phase is TTTTGTG'T, where each letter represents a torsion angle along the N-C₁₀ chain: T for a trans conformation, G and G' for gauche conformations with opposite torsion angles. Accordingly, we modelled the decylammonium ion as a rigid body with ideal 180° and ±60° torsion angles, this time

also fixing the bond lengths and angles. The N atom and free Cl atom were fixed on the plane, while all other atoms were modelled as split sites above and below the plane. Isotropic ADPs were refined for all atoms, with those of N and all C atoms constrained to be the same. Again, H atoms were placed by geometry, and a spherical harmonic correction for preferred orientation was used, refining terms up to eighth order. This model gave excellent agreement with the data.

As a check, we also considered the low-temperature conformation TGTTTTTT and the all-trans possibility TTTTTTTT. These gave poorer fits to the data, although they were individually plausible, indicating the limited sensitivity of powder X-ray diffraction data to the precise conformation of the alkyl chains. For this reason, we made no attempt to model any conformational disorder. However, the rather large ADPs suggest that a more sophisticated disorder model might be preferable if more data were available: for instance, from single-crystal measurements.

This information has now been included in the Supplementary Material, along with a new figure with the refined patterns (Figure S1 in the Supplementary Material) and the low- and high-temperature structures projected on (100) and (010) planes (Figure S2 in the Supplementary Material).

Reviewer's Comment:

2. There are some embarrassing errors about the chemical formula of A2BX4 perovskites, i.e. MCl⁺, (n-CnH2n+1NH3)²⁻. Please double check the expressions in the whole text.

Response: We thank the Reviewer for pointing out these errors, which have been corrected in the new version of the manuscript.

Reviewer's Comment:

3. How did the authors determine the values of such small pressure, such as 0.03, 0.05 GPa?

Response: The pressure was measured using a high-pressure transducer Model HP from Honeywell attached to the high-pressure circuit, which allows the measurement of pressures with a 0.5% accuracy (precision of < 0.001 GPa). This information has now been included in the Experimental Section of the manuscript.

Reviewer's Comment:

4. There are some more studies about the barocaloric effects of hybrid perovskites, the authors should include another important work in Figure 7 (DMAMg(HCOO)₃, DOI: 10.1063/1.5049116); in addition, another related work could be included (DOI: 10.1021/acs.jpcc.9b06169).

Response: In the new version of the manuscript we have included the compound data for the DMAMg(HCOO)₃ in the revised Figure 7.

On the other hand, the following references have been included in the Introduction section:

- M. Szafranski, W.-J. Wei, Z.-M. Wang, W. Li, A. Katrusiak, APL Mater. 2018, 6 100701.

- Y. Qin, Z. Lv, S. Chen, W. Li, Wei, X. Wu, L. Ye, N. Li, P. Lu, J. Phys. Chem. C 2019, 123 22491.

Reviewer's Comment:

5. Some format problems of refs, i.e. refs 6, 28, 29, 30.

Response: The format of the references has been revised and corrected (e.g. abbreviation of journal names)

LIST OF CHANGES

- In addition to changes associated with the Reviewers' Comments as mentioned in our responses, we have performed the following changes in the manuscript:

- While the notation " $(n-C_nH_{2n+1}NH_3)_2MCl_4$ " for the compound under study has been used in the literature (e.g. V. Busico et al., Solar Energy 1980, 24 575-579), we prefer to replace it by the simpler notation " $(C_nH_{2n+1}NH_3)_2MCl_4$ " to avoid any confusion, which is also used in literature (e.g. F. Guillaume et al., Mol. Phys. 1989, 67 665-679).

- The sentence in the introduction "Compounds with M = Mn, Fe (and other very similar compounds), awakened further interest due to their low-dimensional magnetic properties [11, 12, 13, 14]" has been moved from the end of the fourth paragraph to the end of the second paragraph to link better with the new sentence included following a suggestion from the Reviewers.

- The x-axis in Figure 1a was not well vertically aligned with the remaining panels. This has now been corrected.

- Two additional authors have been included in the author list: Anthony E. Phillips and R. Dixey, as they have performed the Rietveld Refinements.

- In the Acknowledgments Section, a sentence related to funding of the two additional coauthors has been included.

- Reference [1] has been updated.

At the end of the "Response Letter to Reviewers.pdf" file we also provide the revised manuscript with changes highlighted (except those small changes related to the language improvement and to the numbering and format of references, and few typos).



Department of Physics
Av. Eduard Maristany 10-14, 08019 Barcelona
Spain
+34 93 4010824
pol.lloveras@upc.edu

July 16th, 2021

Dear Editor,

We hereby submit a revised version of the manuscript entitled “Colossal reversible barocaloric effects in layered hybrid perovskite $(C_{10}H_{21}NH_3)_2MnCl_4$ under low pressure near room temperature”. We really appreciate the time and effort the Reviewers have devoted to our manuscript and thank their comments very much, which have helped to improve it. We are also very pleased to see that both give a positive assessment of our work and consider it worthy for publication after minor changes. In this resubmission we provide a point-by-point response to the Reviewers’ comments with the manuscript with changes highlighted. We hope that our revised manuscript will now be considered suitable for publication in Advanced Functional Materials.

Sincerely yours,

On behalf of all co-authors



Dr. Pol Lloveras

POINT-BY-POINT RESPONSE TO REVIEWERS

REVIEWER #1

Reviewer's Comment:

It is impressive that the compound (C₁₀H₂₁NH₃)₂MnCl₄ performs better BC effects when compared with other BC materials. Therefore, this study presents a good example for developing colossal barocaloric materials. Overall, I suggest that this work can be potentially as a good contribution to Advanced Functional Materials upon further revision.

Response: We thank the Reviewer for his/her positive assessment of our work.

Reviewer's Comment:

1. Authors should demonstrate the detailed processes of obtaining the structural information for the compound (C₁₀H₂₁NH₃)₂MnCl₄, rather than just citing references.

Response: In the revised version of the manuscript, Rietveld refinement has now been performed to determine the high- and low-temperature structures. The corresponding CIFs have been uploaded to CCDC as usual (CCDC numbers 2096682 and 2096683) and the details have been included in the Supplementary Material.

Reviewer's Comment:

2. What is the yield of the chemical reaction? Please provide the synthetic yield of the compound (C₁₀H₂₁NH₃)₂MnCl₄.

Response: We prepared our target sample through the following reaction:



The synthetic yield of the reaction is 90%. However, the as-prepared powder sample needs to be washed and recrystallized from ethanol. The yield of the recrystallizing step is 80%, which depends on the (controllable) cooling speed. Thus, considering the multi-step reaction, the total yield of the compound is *total yield (%)* $\approx (0.9 \cdot 0.8) \cdot 100 \approx 72\%$. This value has now been included into the Experimental Section.

Reviewer's Comment:

3. In Figure S3, the unit cell volume would expand gradually when the temperature increases under the first situation (blue dots), which may be related to the thermal expansion. However, under the second situation (red dots), the volume shows shrinkage as the temperature

increases, which is hard to understand and learn. Please give some explanations.

Response: As mentioned in our response to Reviewer's Comment #1, in the revised version of the manuscript, Rietveld refinement has now been performed to determine the high- and low-temperature structures, whose details have been included in the Supplementary Material. From the obtained structures, pattern matching of the temperature-dependence patterns has been performed to determine the temperature-dependence of the lattice parameters (Figure S4 of the Supplementary Material). While for the low-temperature phase the same results have been obtained as compared to those previously calculated, for the high-temperature phase the resulting dependence of volume on temperature shows a smooth increase with a small thermal expansion coefficient $\alpha_V = 7 \cdot 10^{-5} \text{ K}^{-1}$. Importantly, this is fully consistent within error with the entropy curves calculated previously because the latter are calculated using $\left(\frac{\partial V}{\partial T}\right)_p$ in the low-temperature phase and because in the high-temperature phase the small and positive value for $\left(\frac{\partial V}{\partial T}\right)_p$ yields isothermal entropy changes outside the transition that are very small as compared to the changes occurring at the transition, and negative in sign upon a pressure increase (see Figure 4a,b in the manuscript).

On the other hand, lattice parameter b is observed to undergo a shrinkage upon increasing temperature. While the study of this behavior is beyond the scope of this work, it is worth mentioning that this feature has been observed in other layered perovskites (Huang et al., *Phys. Rev. Lett.* **2016**, *117* 115901) as well as in non-layered perovskites (Shang et al., *Chem. Eur. J.* **2014**, *20* 1146).

Notice also that the number of formula units per unit cell $Z = 4$ was used by mistake, which has now been corrected ($Z = 2$) (panel (e) of Figure S4).

Reviewer's Comment:

4. How about the thermal stability of the compound (C₁₀H₂₁NH₃)₂MnCl₄? Please illustrate.

Response: The compound has shown to be thermally stable along several years after synthesis, being stored without any particular condition. On the other hand, we have also observed that the thermodynamic transition properties are not modified after thermal cycling across the phase transition at different pressures applied randomly. In this sense, our observations are fully consistent with the findings in C. R. Raj et al., "Manganese-based layered perovskite solid–solid phase change material: Synthesis, characterization and thermal stability study", *Mech. Mater.* **2019** *135* 88-97, where the thermal stability of (C₁₀H₂₁NH₃)₂MnCl₄ was specifically investigated.

Reviewer's Comment:

5. To better observe the temperature-dependent spectral changes, authors should point out and mark the characteristic peaks or bands in the Raman spectra (Figure 2a-d).

Response: Following the Reviewer advice, we have included dashed lines indicating the characteristic peaks and explanatory key words in Figures 2a-d.

Reviewer's Comment:

6. *The classical perovskite usually has the structures of ABO₃ or A₂BO₆, so if the hybrid in this work is labeled as perovskite, authors need to discuss more about the perovskite structures.*

Response: The structure of the hybrid studied in this work does not exhibit the true perovskite structure ABO₃, which consists of a 3D corner-sharing octahedra. Instead, compounds such as those with general formula (R-NH₃)₂BX₄ [R-NH₃⁺ = interlayer alkylammonium chain cations, B = divalent metal and X₄²⁻ = halide anions], are called layered perovskites because they exhibit a perovskite-like structure projected on a reduced dimensionality, consisting of corner-sharing BX₆ octahedra in 2 dimensions that form inorganic sheets in the (ab) planes. In this case, the length of the interlayer organic chain prevents the 3D corner-sharing along the c axis between octahedra belonging to different layers, as it does occur in true perovskites. Clear descriptions of the 2D perovskite structures and their relation to 3D true perovskites can be found in the following references:

- Cauê F. Ferreira, PhD Thesis, *Controlling the thermodynamic phase stability of hybrid perovskites with organic media*, University of Florida (2016)
- L. Mao, C. C. Stoumpos, M. G. Kanatzidis, Two-Dimensional Hybrid Halide Perovskites: Principles and Promises, *J. Am. Chem. Soc.* 2019, 141, 1171–1190.
- D. B. Mitzi, Templating and structural engineering in organic–inorganic perovskites, *J. Chem. Soc., Dalton Trans.*, 2001, 1–12.

To make this point clearer in the revised version of the manuscript, we have modified the text and included the two last references above.

Reviewer's Comment:

7. *Following comment 6, in my view, hybrid perovskites and metal organic halides are hot topics in materials science, to arouse a broad interest from readership in this field, several strongly related works on hybrid perovskites materials (*Angew. Chem. Int. Ed.* 2019, 58, 15128; *Chem. Soc. Rev.*, 2021, 50, 5564) and structural and property modulation of metal organic halides (*Adv. Mater.* 2021, 33, 2007571; *Nat. Commun.* 2020, 11, 4649) can be enriched as references.*

Response: Following the Reviewer's advice, we have included the first two references in the Introduction's section. We prefer to leave out the other two as they are particular cases not directly linked with our work.

Reviewer's Comment:

8. The language of this manuscript could be further polished.

Response: Following the Reviewer's comment, the text has been improved.

REVIEWER #2

Reviewer's Comment:

This work is a nice advance in the field of barocalorics materials. The characterizations are comprehensive and the results are convincing. Therefore, I have no doubt to recommend its publication in Advanced Functional Materials provided that the authors can address the following a few minor points:

Response: We really appreciate the Reviewer for his/her very positive assessment of our work.

Reviewer's Comment:

1. The high- and low-temperature structures of (C10H21NH3)2MnCl4 should be provided to facilitate the readers' understanding.

Response: Following the Reviewer suggestion, in the revised version of the manuscript the diffraction patterns of the low-temperature phase at 295 K and of the high-temperature phase at 330 K were refined by means of a Rietveld refinement procedure (Rietveld, J. Appl. Crystallogr. **1969**, 2 65-71), using TOPAS-Academic v.7 (A. A. Coelho J. Appl. Cryst. **2018**, 51 210). Because of this task, Richard Dixey and Anthony E. Phillips have been included in the author list.

In the low-temperature phase, we refined a model based on the reported structure in space group $P2_1/a$. The decylammonium ion was modelled as a rigid body in which all C-C bond lengths and C-C-C bond angles were fixed, while the C-C-C-C torsion angles refined freely. H atoms were placed by geometry. The positions of the Cl atoms were restrained so that the Mn-Cl bond lengths had approximately their reported values of 2.485 and 2.584 Å and the Cl-Mn-Cl angles were approximately 90%. The Mn atom sits on the center of symmetry at the origin and has no translational degrees of freedom. Isotropic atomic displacement parameters (ADPs) were refined for all atoms, with the Cl atoms and, separately, the C and N atoms constrained to have the same value. A spherical harmonic correction for preferred orientation was used, refining terms up to eighth order. This gave good agreement with the experimental data (see Figure S1b in the revised Supplementary Material).

To our knowledge, no structural model of the high-temperature phase has previously been reported. Since the transition is first-order, the space group of this phase is not required to be a supergroup of that of the low-temperature phase. However, for simplicity, and by analogy with the related Cd-containing material (R. Kind et al., J. Chem. Phys. **1979**, 71 2118), we began by

considering possible space groups among the minimal supergroups of $P2_1/a$. These can be divided into two categories: the translationengleiche supergroups, which have orthorhombic symmetry; and the klassengleiche supergroups, which have a new translational symmetry element.

Considering the first possibility, we searched for a possible orthorhombic cell, using simulated annealing to refine the cell parameters in a Pawley fit. It quickly became clear that the experimental pattern could not be reproduced by an orthorhombic cell with the same volume, ruling out the possibility of describing it in a translationengleiche supergroup. On the other hand, a monoclinic cell described it well.

Turning to the second possibility, the obvious potential new translational symmetry element is along the vector $(1/2, 1/2, 0)$, connecting the two Mn atoms. This is easily described by a C-centered cell. There are now only two possible space groups, $C2/m$ and $C2/c$. By inspection, of these only $C2/m$ is compatible with the observed structure (with cell vectors remaining the same as $P2_1/a$).

As a final alternative, we also considered a non-supergroup structure in $Pbca$, in which the unit cell doubles along the c axis. This structure occurs in the Pb analogue of this material (A. Lemmerer, D. G. Billing, Dalton Trans. **2012**, 41 1146). Considering only the peak positions in a Pawley fit showed that this is indeed a plausible unit cell. However, in Rietveld refinement the structural model gave very poor agreement with the data. We did not, therefore, pursue it further.

We concluded therefore that the best description of these data is given by a $C2/m$ model. In this space group, the Mn and one Cl atom must sit on special positions, and have no translational degrees of freedom in Rietveld refinement. The other Cl atom and the decylammonium ion sit on, or are disordered about, the mirror plane. QENS measurements (F. Guillaume et al., Mol. Phys. **1989**, 67 665) suggest that the dominant conformation in the HT phase is TTTTGTG'T, where each letter represents a torsion angle along the N–C10 chain: T for a trans conformation, G and G' for gauche conformations with opposite torsion angles. Accordingly, we modelled the decylammonium ion as a rigid body with ideal 180° and $\pm 60^\circ$ torsion angles, this time also fixing the bond lengths and angles. The N atom and free Cl atom were fixed on the plane, while all other atoms were modelled as split sites above and below the plane. Isotropic ADPs were refined for all atoms, with those of N and all C atoms constrained to be the same. Again, H atoms were placed by geometry, and a spherical harmonic correction for preferred orientation was used, refining terms up to eighth order. This model gave excellent agreement with the data.

As a check, we also considered the low-temperature conformation TGTTTTTT and the all-trans possibility TTTTTTTT. These gave poorer fits to the data, although they were individually plausible, indicating the limited sensitivity of powder X-ray diffraction data to the precise conformation of the alkyl chains. For this reason, we made no attempt to model any conformational disorder. However, the rather large ADPs suggest that a more sophisticated disorder model might be preferable if more data were available: for instance, from single-crystal measurements.

This information has now been included in the Supplementary Material, along with a new figure with the refined patterns (Figure S1 in the Supplementary Material) and the low- and high-temperature structures projected on (100) and (010) planes (Figure S2 in the Supplementary Material).

Reviewer's Comment:

2. There are some embarrassing errors about the chemical formula of A_2BX_4 perovskites, i.e. MCl^+ , $(n-CnH_{2n+1}NH_3)_2^-$. Please double check the expressions in the whole text.

Response: We thank the Reviewer for pointing out these errors, which have been corrected in the new version of the manuscript.

Reviewer's Comment:

3. How did the authors determine the values of such small pressure, such as 0.03, 0.05 GPa?

Response: The pressure was measured using a high-pressure transducer Model HP from Honeywell attached to the high-pressure circuit, which allows the measurement of pressures with a 0.5% accuracy (precision of < 0.001 GPa). This information has now been included in the Experimental Section of the manuscript.

Reviewer's Comment:

4. There are some more studies about the barocaloric effects of hybrid perovskites, the authors should include another important work in Figure 7 (DMAMg(HCOO)₃, DOI: 10.1063/1.5049116); in addition, another related work could be included (DOI: 10.1021/acs.jpcc.9b06169).

Response: In the new version of the manuscript we have included the compound data for the DMAMg(HCOO)₃ in the revised Figure 7.

On the other hand, the following references have been included in the Introduction section:

- M. Szafranski, W.-J. Wei, Z.-M. Wang, W. Li, A. Katrusiak, APL Mater. **2018**, 6 100701.
- Y. Qin, Z. Lv, S. Chen, W. Li, Wei, X. Wu, L. Ye, N. Li, P. Lu, J. Phys. Chem. C **2019**, 123 22491.

Reviewer's Comment:

5. Some format problems of refs, i.e. refs 6, 28, 29, 30.

Response: The format of the references has been revised and corrected (e.g. abbreviation of journal names)

LIST OF CHANGES

- In addition to changes associated with the Reviewers' Comments as mentioned in our responses, we have performed the following changes in the manuscript:

- While the notation " $(n\text{-C}_n\text{H}_{2n+1}\text{NH}_3)_2\text{MCl}_4$ " for the compound under study has been used in the literature (e.g. V. Busico et al., *Solar Energy* **1980**, 24 575-579), we prefer to replace it by the simpler notation " $(\text{C}_n\text{H}_{2n+1}\text{NH}_3)_2\text{MCl}_4$ " to avoid any confusion, which is also used in literature (e.g. F. Guillaume et al., *Mol. Phys.* **1989**, 67 665-679).

- The sentence in the introduction "Compounds with $M = \text{Mn, Fe}$ (and other very similar compounds), awakened further interest due to their low-dimensional magnetic properties [11, 12, 13, 14]" has been moved from the end of the fourth paragraph to the end of the second paragraph to link better with the new sentence included following a suggestion from the Reviewers.

- The x-axis in Figure 1a was not well vertically aligned with the remaining panels. This has now been corrected.

- Two additional authors have been included in the author list: Anthony E. Phillips and R. Dixey, as they have performed the Rietveld Refinements.

- In the Acknowledgments Section, a sentence related to funding of the two additional coauthors has been included.

- Reference [1] has been updated.

Below we provide the revised manuscript with changes highlighted (except those small changes related to the language improvement and to the numbering and format of references, and few typos).

Colossal reversible barocaloric effects in layered hybrid perovskite $(\text{C}_{10}\text{H}_{21}\text{NH}_3)_2\text{MnCl}_4$ under low pressure near room temperature

Junning Li* María Barrio David J. Dunstan Richard Dixey Xiaojie Lou Josep-Lluís Tamarit Anthony E. Phillips Pol Lloveras*

Junning Li

Prof. David J. Dunstan

Dr. Richard Dixey

Dr. Anthony E. Phillips

School of Physics and Astronomy, Queen Mary University of London, London E1 4NS, United Kingdom
junning.li@qmul.ac.uk

Prof. Xiaojie Lou

Frontier Institute of Science and Technology, State Key Laboratory for Mechanical Behavior of Materials, Xi'an Jiaotong University, Xi'an 710049, China

Dr. María Barrio

Prof. Josep Lluís Tamarit

Dr. Pol Lloveras

Grup de Caracterizació de Materials, Departament de Física, EEBE and Barcelona Research Center in Multiscale Science and Engineering, Universitat Politècnica de Catalunya, Eduard Maristany, 10-14, 08019 Barcelona, Catalonia. pol.lloveras@upc.edu

Keywords: *Barocaloric effects, hybrid layered perovskites, calorimetry, phase diagram, Raman scattering*

We report barocaloric effects in a layered hybrid organic-inorganic compound, $(\text{C}_{10}\text{H}_{21}\text{NH}_3)_2\text{MnCl}_4$, that are reversible and colossal under pressure changes below 0.1 GPa. This barocaloric performance originates in a phase transition characterized by different features: A strong disordering of the organic chains, a very large volume change, a very large sensitivity of the transition temperature to pressure and a small hysteresis. Our obtained values are unprecedented among solid-state cooling materials at such low pressure changes and demonstrate that colossal effects can be obtained in compounds other than plastic crystals. The temperature-pressure phase diagram displays a triple point indicating enantiotropy at high pressure.

1 Introduction

In recent years, research on caloric effects induced by changes in applied hydrostatic pressure has experienced a significant growth [1], boosted by the urgent need of replacing hydrofluorocarbon-based devices that currently cause around $\sim 8\%$ of global greenhouse emissions [2]. A milestone has recently been achieved by the discovery of colossal barocaloric (BC) effects in plastic crystals [3, 4]. While these materials seem to represent an upper limit for the isothermal entropy changes, there is still room for improvement in terms of reducing the required pressure changes to obtain reversible barocaloric effects useful for real devices. Other systems such as hybrid organic-inorganic perovskites (HOIPs) [5, 6] and spin-crossover compounds [7] have revealed large reversible adiabatic temperature changes at moderate pressures along with giant isothermal entropy changes within large temperature spans, yielding excellent performance as BC agents thanks to phase transitions with small hysteresis and extreme sensitivity to pressure.

The extraordinary chemical flexibility in HOIPs allows a diversity of combinations that can be explored to tune their properties, seek optimal operational regimes and maximize performance. Indeed, HOIPs have raised great expectations in diverse areas of materials science due to their multifunctional properties, as used in photovoltaic technologies and optoelectronics [8]. Within such rich compositional and structural variety, an HOIP subfamily with the chemical formula $(\text{C}_n\text{H}_{2n+1}\text{NH}_3)_2\text{MCl}_4$ ($n = 1, 2, 3, \dots$), with M being a divalent metal, attracted particular interest in the 1970's [9] as phase change materials for thermal energy storage applications. As in the case of plastic crystals [10], this functionality emerges due to the occurrence of highly energetic, fully reversible first-order phase transitions with suitable transition temperatures. This feature, along with a large transition volume change, suggests that these com-

pounds could be very suitable as barocaloric agents, as plastic crystals have already shown. Compounds with $M = \text{Mn, Fe}$ (and other very similar compounds), awakened further interest due to their low-dimensional magnetic properties [11, 12, 13, 14] whereas other layered HOIPs are being investigated for photoluminescence properties [15, 16, 17].

As in plastic crystals, the huge latent heat originates in the dynamic structural disorder released across the transition. However, in contrast to the orientational disorder facilitated globular or small molecules in plastic crystals, $(\text{C}_n\text{H}_{2n+1}\text{NH}_3)_2\text{MCl}_4$ compounds exhibit more complex structure and dynamical disorder. In particular, their structure has a 2-dimensional layered symmetry similar to lipid bilayers, displaying a perovskite-like structure of reduced dimensionality with MCl_6 octahedra sharing their corners only between neighbors in the (ab) planes. Between these planes there are two chains of alkylammonium $\text{C}_n\text{H}_{2n+1}\text{NH}_3^+$ cations arranged along the c direction, whose length prevents the 3D corner-sharing along this axis between octahedra belonging to different layers, as it does occur in true perovskites [18, 19]. These chains are linked at the ammonium end to the inorganic octahedra by electrostatic interactions and hydrogen bonds. The organic chain tails facing each other are stabilized by their van der Waals interactions [20, 21].

Often, these compounds show rich polymorphism already at atmospheric pressure, typically displaying a sequence of two (sometimes more) transitions, one being significantly more energetic [9, 22, 23]. At this major transition, while the organic chain remains ionically bonded to the inorganic part [24], some gauche conformations arise in the alkyl bonds, which show dynamic mobility along the chain. This so-called chain-melting process is at the origin of the huge entropy changes at the transition. The emergence of the gauche conformations causes the chains to shorten. However, this is more than compensated by the increase of the distance between the ends of the facing chains, leading to a significant positive net volume change. The minor transition is order-disorder, where the disorder was concluded to consist of the rigid chains rotating around the longitudinal chain axis between two equivalent orientations separated by 90° , and with neighboring chains rotating in opposite directions. While not as enormous as the major transition entropy change, the entropy change at the minor transition is still giant. The sequence of these transitions is not unique; it may vary from one composition to another. The transition temperatures increase with increasing n , which is consistent with the enhancement of the stability regime of the ordered phase with the increasing chain length, that will be more difficult to destabilize. From $n = 9$ to $n = 17$ the transition temperature varies from 287 K to 373 K, thus offering a range of compositions with caloric effects near room temperature.

Here we choose the compound $(\text{C}_{10}\text{H}_{21}\text{NH}_3)_2\text{MnCl}_4$ [$n = 10$, 10-bis(alkylammonium) tetrachloromanganate(II), C_{10}Mn for short] because in this material the disorder fully develops across a single phase transition and near room temperature and therefore exhibits a larger transition entropy change than compounds with larger n values. Using pressure-dependent calorimetry and X-ray diffraction, we demonstrate not only that colossal barocaloric effects can be obtained in compounds other than plastic crystals, such as this layered HOIP family, but also that an improved BC performance can be obtained at lower pressure than those reported so far in plastic crystals, due to a very small hysteresis and a very large sensitivity of the transition temperature to pressure. Raman scattering experiments explore changes in structure and dynamics across the transition.

2 Results and discussion

2.1 Structural and thermodynamic properties at atmospheric pressure

The structure of C_{10}Mn was characterized using X-ray powder diffraction (XRDP) measurements at atmospheric pressure and at temperatures around its solid-to-solid first-order phase transition. The diffraction patterns of the low-temperature phase at 295 K and of the high-temperature phase at 330 K were refined by means of a Rietveld refinement procedure [25] using TOPAS-Academic v.7 [26]. At low temperatures, a $P2_1/a$ structure (cif number: CCDC 2096682) was obtained, consistent with that reported

in Ref. [27], and in disagreement with the orthorhombic structure reported in Ref. [21]. For the high-temperature phase, which was previously undetermined, a $C2/m$ structure was obtained (cif number: CCDC 2096683). From these refinements, pattern matching of the temperature dependent XRDP patterns was performed, to obtain the unit cell volume as a function of temperature $V(T)$ (see Fig. 1a). This revealed a very large increase in volume at the endothermic transition of $\Delta V_t/V_{II} \sim 7\%$. A thorough explanation of the refinement details, the crystallographic structures of the unit cell in the two phases and the dependence of the patterns and the lattice parameters on temperature can be found in the Supplementary Material.

Isobaric temperature-dependent calorimetry at atmospheric pressure yielded positive and negative peaks in $dQ/|dT|$ associated with endothermic and exothermic first-order phase transitions, respectively (see Figure 1b). The maxima of the peaks were obtained at $T_{II \rightarrow I} = 312 \pm 1$ and $T_{I \rightarrow II} = 303 \pm 1$, whereas the onsets of the peaks at $T_{II \rightarrow I} = 309 \pm 1$ K and $T_{I \rightarrow II} = 306 \pm 1$ K. This shows a hysteresis of ~ 9 K as defined from the peak maxima, and ~ 3 K as defined from the peak onsets, which are both small. Integration over temperature of $dQ/|dT|$ and $(1/T)dQ/|dT|$ after baseline subtraction yielded transition enthalpy changes $\Delta H_{II \rightarrow I} = 76 \pm 4$ J g $^{-1}$ and $\Delta H_{I \rightarrow II} = 79 \pm 4$ J g $^{-1}$ and transition entropy changes $\Delta S_{II \rightarrow I} = 241 \pm 12$ J K $^{-1}$ kg $^{-1}$ and $\Delta S_{I \rightarrow II} = 261 \pm 13$ J K $^{-1}$ kg $^{-1}$, in very good agreement with the literature [27, 28]. The integrated curve for ΔS_t was used with the temperature-dependent heat capacity C_p obtained from modulated calorimetry (see Fig. 1c) to calculate the temperature-dependent entropy with respect to a reference temperature $T_0 = 213$ K (chosen arbitrarily below the transition) as $S(T, p_{\text{atm}}) - S(T_0, p_{\text{atm}}) = \int_{T_0}^T \frac{1}{T} (C_p + dQ/dT) dT$ (see Fig. 1d).

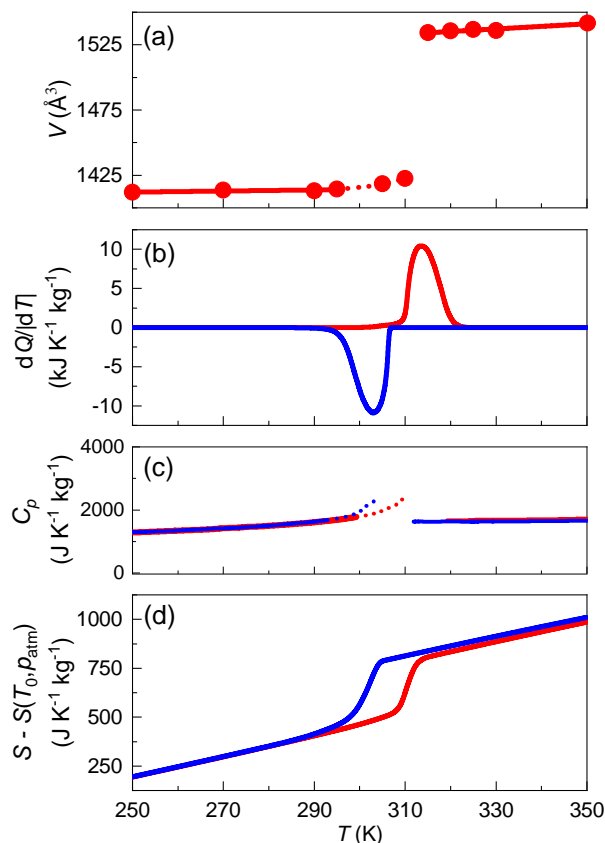


Figure 1: (a) Unit cell volume, (b) heat flow in temperature, (c) specific heat and (d) isobaric entropy as a function of temperature at atmospheric pressure. Red and blue curves correspond to data obtained on heating and on cooling, respectively.

To understand the origin of such large entropy changes at the transition, we investigated the molecular disordering process by temperature-dependent Raman scattering in both low and high wavenumbers. Previous Raman studies on organic chains have described a peak at low frequency as corresponding to

an accordion-like longitudinal acoustic mode (LAM) [29, 30, 31]. In our measurements, such a peak is obtained in the low temperature phase near 235 cm^{-1} (see Figure 2a). In particular, this is higher than the value for all-trans (T) chain (209 cm^{-1}) or for chains of the same length engaged in hydrogen bonds, such as n-decylamine (213 cm^{-1}) or decylammonium chloride (217 cm^{-1}) [32], and corresponds to a conformational effect and the existence of a gauche (G) conformation near the NH_3 polar head. In Fig. 2b, the characteristic bands of the trans planar chains are observed at $1065, 1109, 1146$ and 1174 cm^{-1} . This indicates that the most intense bands in the Raman spectrum of the long alkyl chains correspond to the limiting $k = 0$ modes of an infinite chain [33]. Figures 2c and 2d show the characteristic bands of the C-H twisting (1300 cm^{-1}), bending ($1420\text{-}1480\text{ cm}^{-1}$) and stretching ($2830\text{-}3000\text{ cm}^{-1}$) mode. It is worth noting that the scattering wing on the 2846 cm^{-1} line is due to intermolecular forces [33]. Moreover, the Mn-Cl stretching mode band can be found at 186 and 236 cm^{-1} (overlapped with LAM at 235 cm^{-1}) and wavenumbers $300, 1040$ and 1080 cm^{-1} correspond to the NH_3 torsional band (overlapped with the trans bond stretching at 300 cm^{-1}) [34, 35]. Overall, the low-temperature study of these spectral regions indicates a typical ordered state of the low-temperature phase and gives further evidence for the existence of inter- and intramolecular coupling in an almost completely extended chain. In the high-temperature phase, the Raman spectra indicate the emergence of disorder. Firstly, the LAM mode and the limiting $k = 0$ mode bands disappear and only a broad and weak band is observed near 247 cm^{-1} , which means the conformation of the long trans planar chains is changed. Further evidence of appearing of the gauche bond structure can be found in the decrease of the 1465 cm^{-1} shoulder, which is due to intramolecular coupling of trans structures [33, 35]. In order to fully understand the structure of the organic part, we schematically show the probable conformation of the decylammonium chain as reported in the literature from infrared spectra [27] and incoherent neutron scattering [36]. In Figures 2e and 2f we can see that the conformation for low temperature is T-G-T-T-T-T-T-T while the high temperature becomes T-T-T-T-G-T-G'-T. As discussed previously, it is believed that the reorientation of the whole chain and the disorder of the hydrocarbon parts comes from the increase of the G and G' conformation which is regarded as conformational disorder and contributes a large latent heat in the order-disorder first-order phase transition. Furthermore, the C-H stretching mode bands at $2870, 2883$ and 2930 cm^{-1} merge into a broad scattering peak, indicating that the intermolecular forces were greatly changed. Finally, the Mn-Cl stretching mode bands become weak and broad at high temperature with the disappearing of the NH_3 torsional mode band. This means a dramatic change for the layer, which is consistent with the increase of the *c*-axis length from the XRD data (see Supplementary Figure S4).

2.2 Thermodynamic properties at high pressure

Isobaric temperature-dependent calorimetry performed at selected pressures (see Figure 3a and Supplementary Figure S5) below 0.1 GPa reveals single peaks associated with the $\text{II} \leftrightarrow \text{I}$ transition, that shift strongly to higher temperatures with increasing pressure (see Figures 3b-d). This shift can be fitted by slightly convex second-order polynomials, yielding $\frac{dT_{\text{II} \rightarrow \text{I}}}{dp} = 250 \pm 6\text{ K GPa}^{-1}$ and $\frac{dT_{\text{I} \rightarrow \text{II}}}{dp} = 280 \pm 20\text{ K GPa}^{-1}$ for the endothermic and exothermic transitions, respectively, at atmospheric pressure. Above 0.15 GPa , the endothermic calorimetric signals clearly exhibit two consecutive peaks which indicate the appearance of a new phase (III) between the two peaks. The larger peak corresponds to the transition $\text{II} \rightarrow \text{III}$ and is followed by the smaller peak corresponding to the $\text{III} \rightarrow \text{I}$. The exothermic transitions show the peak splitting at lower pressures. Two possible causes are, (i) the occurrence of transitions between equilibrium phases, I-III-II , but with different hysteresis (i.e. a larger thermal hysteresis of the transition $\text{III} \rightarrow \text{II}$ than that of the transition $\text{I} \rightarrow \text{II}$), for which the peak splitting can be more easily identified in exothermic peaks than in endothermic peaks because in the latter the overlap of the very close peaks prevents distinguishing them; (ii) the occurrence of a metastable phase transition from the equilibrium phase I to the metastable phase III at temperatures and pressures below the triple point in equilibrium, followed by a phase transition from the metastable phase III to the stable phase II. Or a combination of (i) and (ii) is possible. The striking similarity between the $\frac{dT}{dp}$ values of the different coexistence lines ($\frac{dT_{\text{II} \rightarrow \text{III}}}{dp} = 180 \pm 1\text{ K GPa}^{-1}$, $\frac{dT_{\text{III} \rightarrow \text{II}}}{dp} = 161 \pm 2\text{ K GPa}^{-1}$, $\frac{dT_{\text{III} \rightarrow \text{I}}}{dp} = 170 \pm 2\text{ K GPa}^{-1}$, $\frac{dT_{\text{I} \rightarrow \text{III}}}{dp} = 160 \pm 3\text{ K GPa}^{-1}$)

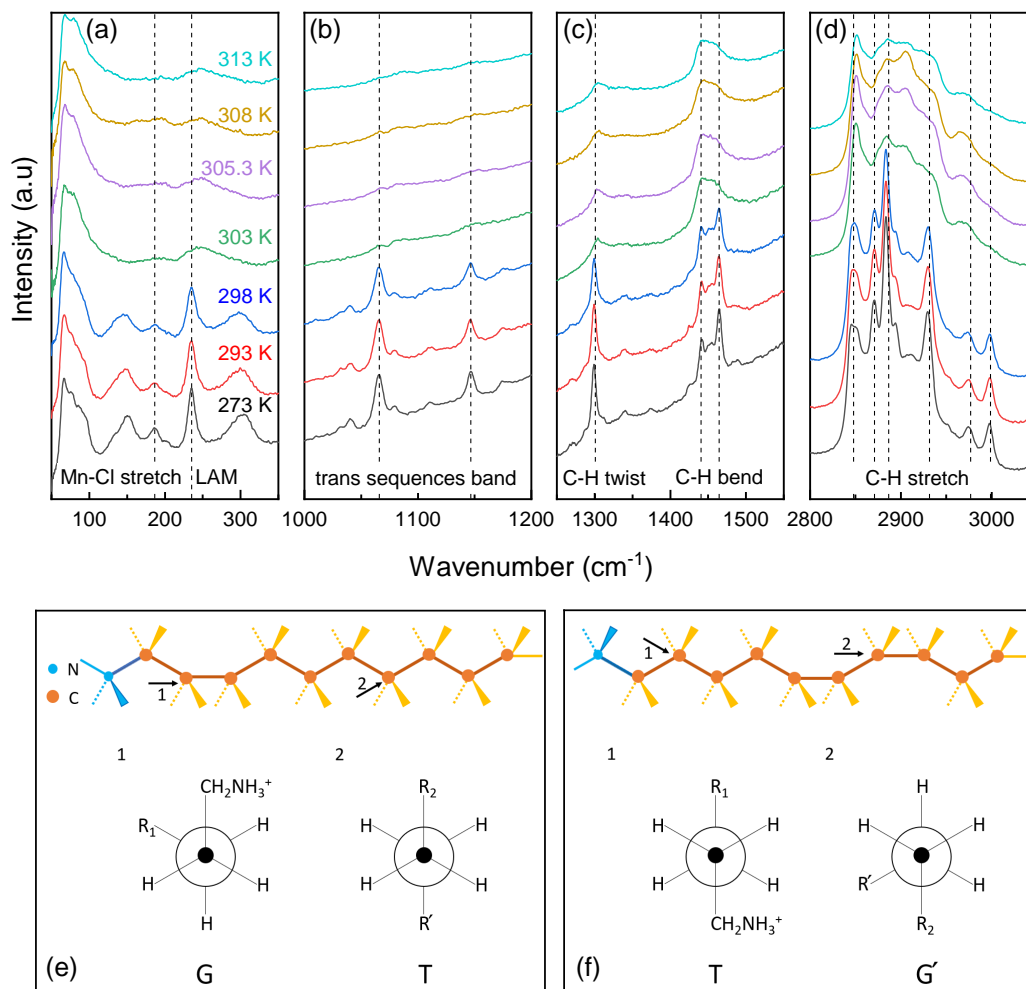


Figure 2: (a-d) Temperature dependence of the Raman spectrum of $(C_{10}H_{21}NH_3)_2MnCl_4$ at different wave number intervals. (e,f) Schematic diagram for the probable conformation of the decylammonium chain under low and high temperature respectively, along with Newman projections for trans (T) and gauche (G) conformations corresponding to the positions indicated by numbers 1 and 2. R_1 stands for $-CH_2-CH_2-CH_2-CH_2-CH_2-CH_2-CH_3$. R_2 stands for $-CH_2-CH_2-CH_2-CH_2-CH_2-CH_2-NH_3^+$. R' stands for $-CH_2-CH_3$.

GPa⁻¹) makes it even more difficult to determine the actual cause. Moreover, this behavior prevents an accurate determination of the coordinates of the triple point where phases I, II and III coexist in equilibrium, (T_{tp}, p_{tp}) , as cause (i) would lead the triple point to be at $(\sim 330 \text{ K}, \sim 0.12 \text{ GPa})$ whereas cause (ii) would lead the triple point to be closer to $(\sim 337 \text{ K}, \sim 0.14 \text{ GPa})$. On the other hand, notice that at the highest applied pressure $p = 0.36 \text{ GPa}$ the exothermic peaks are observed in the inverse order, with first the larger peak followed by the smaller peak. This behavior can only be explained if part of the material undergoes a phase transition from stable phase I towards a metastable phase II, which on further cooling becomes stable, while the rest of the material undergoes the transition sequence between stable phases $I \rightarrow III \rightarrow II$.

Integration of the peaks in $(1/T)(dQ/|dT|)$ at different pressures reveals that the transition entropy change decays significantly with increasing pressure, at a rate of $\sim -1.1 \cdot 10^3 \text{ J K}^{-1} \text{ kg}^{-1} \text{ GPa}^{-1}$ (see Figure 3e). Close to the triple point, we obtained $\Delta S_{II \rightarrow I}(p \sim 0.15 \text{ GPa}) = 144 \pm 14 \text{ J K}^{-1} \text{ kg}^{-1}$, $\Delta S_{II \rightarrow III} = 102 \pm 10 \text{ J K}^{-1} \text{ kg}^{-1}$ and $\Delta S_{III \rightarrow I} = 32 \pm 4 \text{ J K}^{-1} \text{ kg}^{-1}$. For the exothermic transitions we obtained $\Delta S_{II \rightarrow I}(p \sim 0.15 \text{ GPa}) = 196 \pm 20 \text{ J K}^{-1} \text{ kg}^{-1}$, $\Delta S_{II \rightarrow III} = 134 \pm 14 \text{ J K}^{-1} \text{ kg}^{-1}$ and $\Delta S_{III \rightarrow I} = 60 \pm 6 \text{ J K}^{-1} \text{ kg}^{-1}$. Notice that these values are consistent with the thermodynamic requirement at the triple point $\Delta S_{II \rightarrow I} \sim \Delta S_{II \rightarrow III} + \Delta S_{III \rightarrow I}$. By comparison with the transition sequence exhibited by other compounds

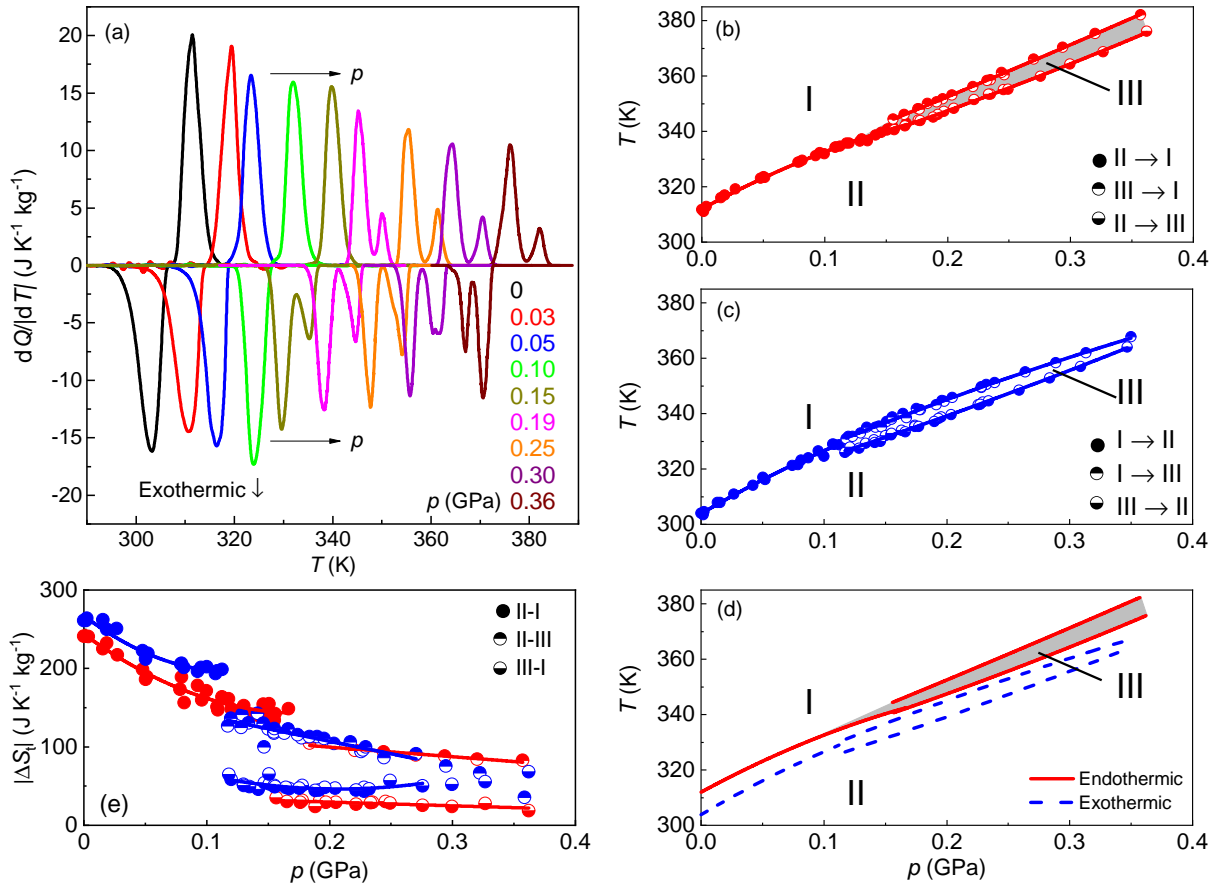


Figure 3: (a) Isobaric heat flow $dQ/|dT|$ as a function of temperature at different applied pressures on heating (positive peaks) and on cooling (negative peaks). (b-d) Transition temperatures as a function of pressure determined as the maximum of the peaks. For the sake of clarity, endothermic (b) and exothermic (c) data are shown separately. Panel (d) shows the fits for both endothermic and exothermic transitions. Shaded areas show the equilibrium region for phase III. (e) Transition entropy change as a function of the applied pressure, for the endothermic (red) and exothermic (blue) transitions. Filled symbols, top-half filled symbols and bottom-half filled symbols stand for $\text{II} \leftrightarrow \text{I}$, $\text{III} \leftrightarrow \text{I}$ and $\text{II} \leftrightarrow \text{III}$ transitions, respectively. Lines are fits to data.

of the same family at atmospheric pressure [9, 22, 23], and given that $\Delta S_{\text{II} \rightarrow \text{III}}$ is significantly larger than $\Delta S_{\text{III} \rightarrow \text{I}}$, we expect that above the triple point the $\text{II} \rightarrow \text{III}$ transition is the major transition involving the chain melting whereas the $\text{III} \rightarrow \text{I}$ transition corresponds to the minor transition of the order-disorder type. On the other hand, given the inverse transition order obtained on cooling in a very few cases, to avoid any inconsistency in the determination of $\Delta S_{\text{I} \rightarrow \text{III}}$ and $\Delta S_{\text{III} \rightarrow \text{II}}$, we have omitted the integration values at high pressure when performing the fits to the data displayed in Figure 3e and when determining the BC effects. Also, it is worth noticing that the joint integration of the two peaks shows a smooth and monotonic behavior regardless of the transition order (see Supplementary Figure S6). This strongly indicates that the transitions order does not affect the thermodynamic properties associated with the overall transition path $\text{I} \rightarrow \text{II}$.

2.3 Determination of entropy as a function of temperature and pressure

To calculate the barocaloric effect via the quasi-direct method, the isobaric entropy as a function of temperature and for different pressures, $S(T, p)$ was obtained with respect to a reference taken at temperature T_0 and atmospheric pressure. The procedure to obtain $S(T, p)$ consisted of integration of a TdS equation for an homogeneous system, extended to include a phase transition contribution, which can be expressed mathematically as:

$$S(T, p) = S(T_0, p_{\text{atm}}) - \int_{p_{\text{atm}}}^p \left(\frac{\partial V}{\partial T} \right)_p dp + \int_{T_0}^T \frac{1}{T'} \left(C_p(T', p) + \frac{dQ}{|dT'|} (T', p) \right) dT'. \quad (1)$$

At $T = T_0$, the integral over temperature vanishes and we obtained $S(T_0, p)$ through an isothermal path from $S(T_0, p_{\text{atm}})$ via the integral over pressure in Eq. 1, which was approximated to $\simeq \left(\frac{\partial V}{\partial T} \right)_{p_{\text{atm}}} p$. Above T_0 , $S(T, p)$ was calculated through the integral over temperature. There, $\frac{dQ}{|dT'|} (T', p)$ is the temperature- and pressure-dependent transition heat flow shown in Figure 3a and $C_p(T', p)$ accounts for the isobaric heat capacity (shown in Supplementary Figure S7). The temperature dependence of C_p in the transition temperature interval was estimated as a weighted average of the two phases I and II, i.e. $C_p(T', p) = (1 - x)C_p^{\text{II}}(T', p) + xC_p^{\text{I}}(T', p)$, where $x(T)$ is the fraction of the system in phase I and is computed using the normalized cumulative integral for the transition entropy change. The former expression is also used for pressures above the triple point, where the C_p of phase III is experimentally inaccessible. However, given the very narrow temperature range of stability of this phase, the error introduced in the entropy due to this approximation is expected to be insignificant.

The pressure dependence of C_p was evaluated from the temperature dependence of the volume by means of the thermodynamic relation $\left(\frac{\partial C_p}{\partial p} \right)_T = -T \left(\frac{\partial^2 V}{\partial T^2} \right)_p$. According to our data, $V(T)$ is approximately linear in phase II below ~ 295 K and in phase I in the measured interval (see red linear fit in Figure 1a), indicating that C_p is independent of pressure in these temperature intervals (red and blue lines in Figure 1c). Instead, $V(T)$ is nonlinear in the temperature interval (295 – 310) K (see dashed line in Figure 1a), indicating a pressure dependence C_p in this temperature interval (see dashed lines in Figure 1c). Moreover, as the transition temperature increases with pressure, these C_p features must be translated to higher temperatures with increasing pressure an amount $(dT/dp)(p - p_{\text{atm}})$. Calculated $C_p(T, p)$ curves are shown in Supplementary Figure S8. A very detailed explanation of the procedure for the construction of the $C_p(T, p)$ curves can be found in Ref. [37]. The resulting functions $S(T, p) - S(T_0, p_{\text{atm}})$ are shown in Figure 4 for selected pressures.

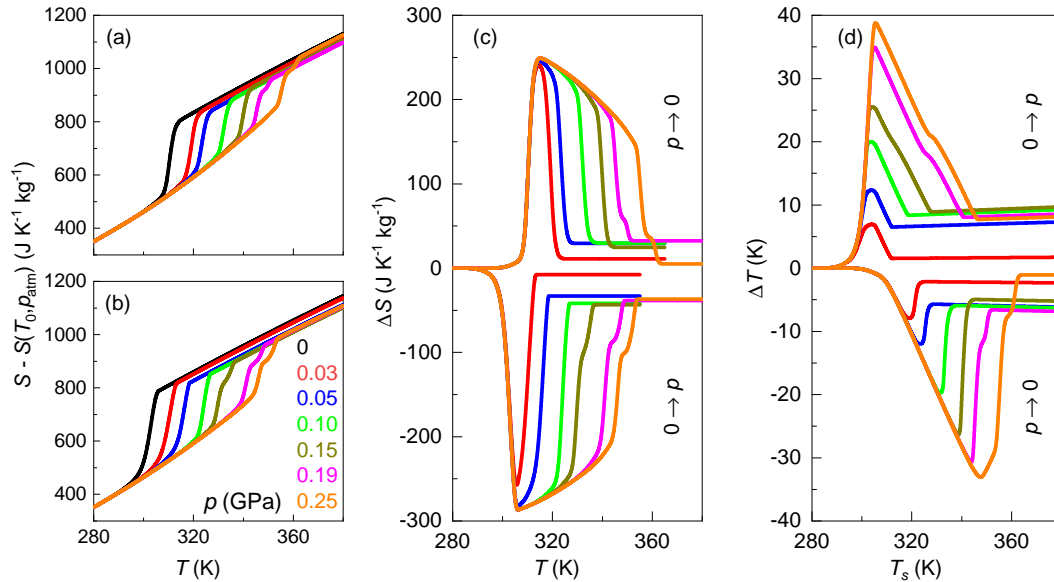


Figure 4: Isobaric entropy as a function of temperature for different values of applied pressure, on heating (a) and on cooling (b). (c) Isothermal entropy changes as a function of temperature and (d) adiabatic temperature changes as a function of the starting temperature, for different values of pressure changes on first compression and on first decompression.

2.4 Barocaloric effects and performance

BC effects were calculated from or to atmospheric pressure so that pressure changes will be approximated to $|\Delta p| \sim p$. For phase transitions with $dT/dp > 0$, transitions on decompression (compression) are endothermic (exothermic) and therefore BC effects, ΔS and ΔT , on first decompression (compression) must be computed from isobaric entropy functions on heating [$S_H(T; p)$] (cooling, [$S_C(T; p)$]), as displayed in Figure 4(a,b). More importantly, this feature entails that the reversible ΔT usable in cooling devices that work in sequential compression–decompression cycles, are given by $|\Delta T_{\text{rev}}(S; p_{\text{atm}} \leftrightarrow p)| = |T_C(S; p) - T_H(S; p_{\text{atm}})|$. In turn, ΔS_{rev} can be determined as the overlapping between $\Delta S(T; p_{\text{atm}} \rightarrow p)$ and $\Delta S(T; p \rightarrow p_{\text{atm}})$. The obtained results (shown in Figure 5a,b) reveal reversible values for ΔS_{rev} that exceed $100 \text{ J K}^{-1} \text{ kg}^{-1}$ under pressure changes as low as 0.03 GPa, and are colossal ($\sim 230 \text{ J K}^{-1} \text{ kg}^{-1}$) under $p \sim 0.05 \text{ GPa}$. Under $p \sim 0.1 \text{ GPa}$, we obtain colossal BC effects of $\Delta S_{\text{rev}} \sim 250 \text{ J K}^{-1} \text{ kg}^{-1}$ and $\Delta T_{\text{rev}} \sim 12 \text{ K}$, with a refrigerant capacity $RC \equiv \int \Delta S_{\text{rev}} dT \sim 3.5 \text{ kJ kg}^{-1}$ (see Figure 5c). Joint values for ΔS_{rev} and ΔT_{rev} are plotted in Figure 6a for different applied pressure changes as a function of temperature. The temperature span where these effects occur near room temperature are plotted as a function of the applied pressure change p in Figure 6b and 6c for ΔS_{rev} and ΔT_{rev} , respectively. For instance, at $p \sim 0.1 \text{ GPa}$, at least $\Delta S \sim 100 \text{ J K}^{-1} \text{ kg}^{-1}$ are obtained within an interval of $\sim 13 \text{ K}$.

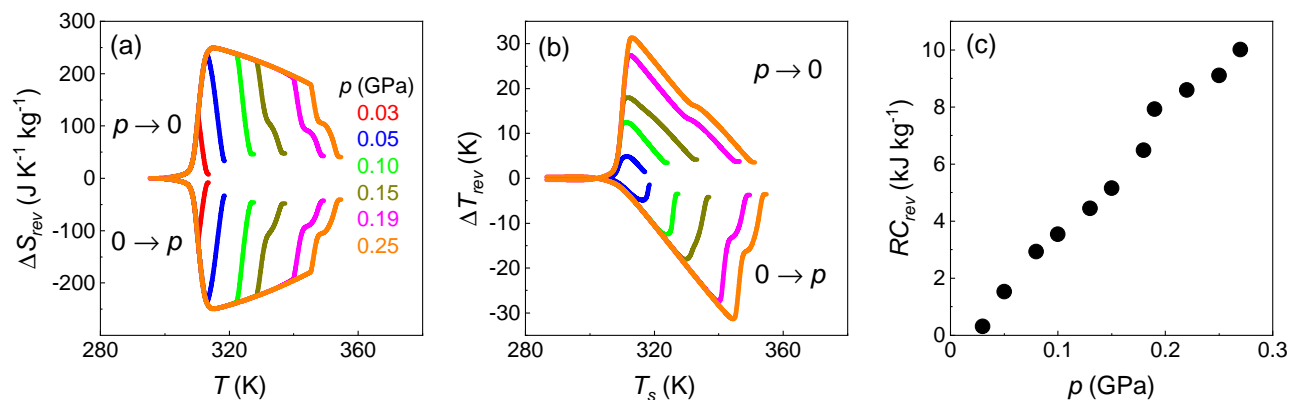


Figure 5: Reversible (a) isothermal entropy changes and (b) adiabatic temperature changes upon application and removal of pressure changes from or to atmospheric pressure, as a function of temperature. (c) Reversible refrigerant capacity as a function of pressure change.

Finally, we calculate the Coefficient of Refrigerant Performance (CRP) [38, 39] for comparison with other BC materials (see Figure 7). The set of values for this compound are comparable to or better than the best reversible BC effects reported so far (e.g. 1-Br-ada and 1-Cl-ada [1, 40]). Particularly interesting is the low pressure change for which these excellent values are obtained, which brings BC materials closer to real applications, such as solid-state cooling or heat pumping. Our study paves the way for finding colossal BC effects in compounds beyond plastic crystals, thus widening the range of suitable materials and stimulating the research in similar compounds. This is especially appealing in this family of compounds because material properties can be sensitively tuned to match desired features by changing the chain length and/or by chemical substitution of the cation.

3 Conclusions

In this work we have demonstrated colossal barocaloric effects in a hitherto unexplored material family, the hybrid organic-inorganic layered perovskites. In particular, $(\text{C}_{10}\text{H}_{21}\text{NH}_3)_2\text{MnCl}_4$ undergoes reversible isothermal entropy changes of $\sim 230 \text{ J K}^{-1} \text{ kg}^{-1}$ under low pressure changes of 0.05 GPa, and reversible adiabatic temperature changes of $\sim 10 \text{ K}$ under pressure changes of 0.08 GPa near room temperature, which are outstanding compared to other solid-state materials. The origin of this extremely good response is a very large increase in entropy and volume associated with the melting of the organic chain

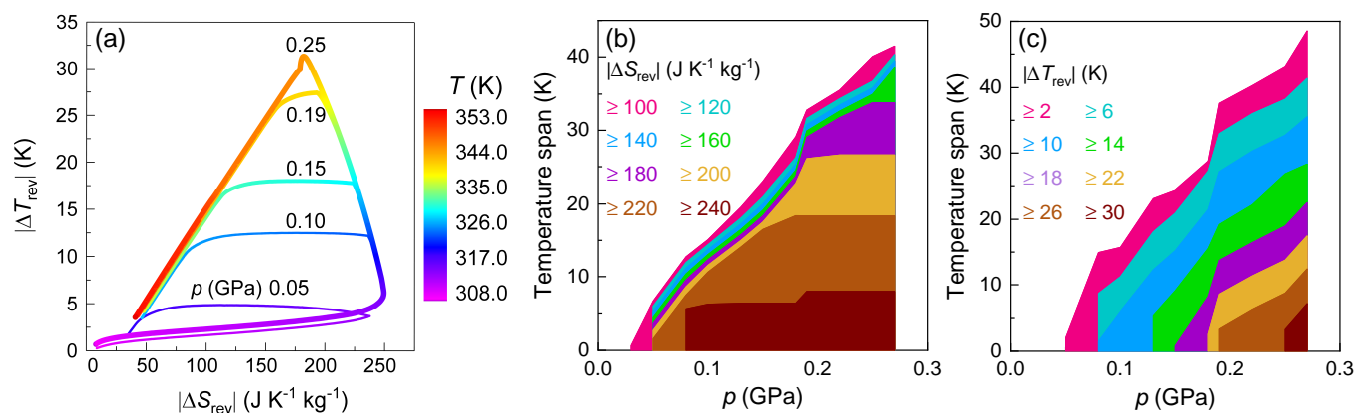


Figure 6: (a) Reversible adiabatic temperature changes and isothermal entropy changes that can be obtained at different applied pressure changes, occurring at temperatures indicated by the color code. Temperature span where a range of (b) isothermal entropy changes and (c) adiabatic temperature changes take place, as a function of the required pressure change.

across a sharp and low-hysteresis first-order solid-solid phase transition. This compound not only widens the horizons for colossal barocaloric materials to include other compounds beyond the canonical plastic crystals but it also expands the limits for the barocaloric performance in solid-state materials. Our results suggest that this compound is among the best candidates to be exploited as a barocaloric agent in pressure-driven solid-state cooling.

4 Experimental Section

Preparation of the sample:

The $(\text{C}_{10}\text{H}_{21}\text{NH}_3)_2\text{MnCl}_4$ sample was prepared by using a two-step reaction method. Manganese(II) chloride tetrahydrate ($\text{MnCl}_2 \cdot 4\text{H}_2\text{O}$, 99%, Sigma Aldrich) was added into hydrochloric acid (HCl , 36.5 to 38.0%, Baker Analyzed) with magnetic stirring until $\text{MnCl}_2 \cdot 4\text{H}_2\text{O}$ was fully dissolved. Then, n-decylamine ($\text{C}_{10}\text{H}_{21}\text{NH}_2$, 99%, ACROS Organics) was added into this mixed solution with magnetic stirring for 3 hours. Then, $(\text{C}_{10}\text{H}_{21}\text{NH}_3)_2\text{MnCl}_4$ powder was obtained by precipitation and washed with ethanol twice.

The total yield of the compound is $\approx 72\%$.

X-ray Diffraction:

X-ray diffraction patterns were obtained using two diffractometers: A Siemens D5000 X-ray Powder diffractometer using monochromatic $\text{Cu-K}_{\alpha 1}$ radiation was employed to check the purity of the synthesized samples because impurities have been reported to modify thermodynamic transition data [22]. An INEL diffractometer with $\text{Cu-K}_{\alpha 1} = 1.5406 \text{ \AA}$ radiation, a curved position-sensitive detector (CPS120), a 0.5-mm-diameter Lindemann capillary and a 700 series Oxford Cryostream Cooler to control the temperature were used to perform temperature-dependent high-resolution X-ray powder diffraction measurements at atmospheric pressure and different temperatures.

Raman Spectroscopy:

Raman spectra were obtained using an IK Series Raman spectroscopy system. A 532 nm He-Cd laser was used for excitation. A calibrated Linkam heating-cooling stage was utilized to control sample temperature, via a thermocouple attached to the sample holder.

Differential scanning calorimetry (DSC):

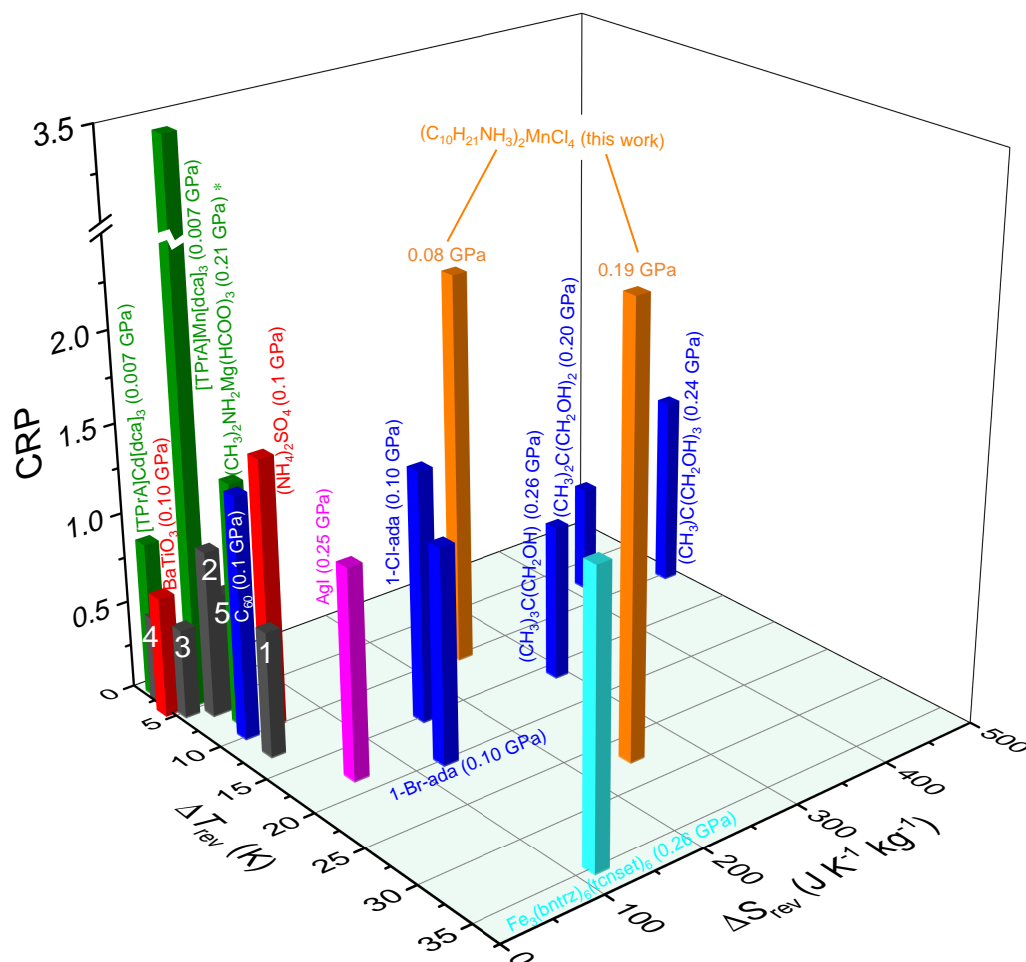


Figure 7: Coefficient of Refrigerant Performance, reversible adiabatic temperature changes and reversible isothermal entropy changes for different materials reported in literature [1]. Label 1 corresponds to $\text{MnCoGeB}_{0.03}$, 2 to $\text{Co}_{50}\text{Fe}_{2.5}\text{V}_{31.5}\text{Ga}_{16}$, 3 to $\text{Fe}_{49}\text{Rh}_{51}$, 4 to $\text{Ni}_{35.5}\text{Co}_{14.5}\text{Mn}_{35}\text{Ti}_{15}$ and 5 to $\text{MnNiSi}_{0.61}\text{FeCoGe}_{0.39}$. Color bars stand for different types of transitions: Black refer to ferromagnetic or metamagnetic systems, cyan to spin-crossover compounds, magenta to superionic conductors, red to ferroelectric inorganic salts, blue to plastic crystals, green to hybrid organic-inorganic perovskites and orange to the hybrid compound studied in this work. *The value of ΔT used for $(\text{CH}_3)_2\text{NH}_2\text{Mg}(\text{HCOO})_3$ is irreversible.

DSC at atmospheric pressure was performed using a Q100 DSC from TA Instruments. A few mg were hermetically encapsulated into the Al capsule sample-holders. Heating and cooling ramps were performed at $\pm 2 \text{ K min}^{-1}$. Measurements of specific heat C_p were performed at atmospheric pressure in a commercial differential scanning calorimeter (DSC, TA Q2000), at 5 K min^{-1} , using $\sim 5 \text{ mg}$ samples of $(\text{C}_{10}\text{H}_{21}\text{NH}_3)_2\text{MnCl}_4$. The amplitude was 0.5 K and period was 60 s . The heating and cooling rate were 2 K min^{-1} .

High-Pressure differential thermal analysis (HP-DTA):

HP-DTA was performed using three different bespoke variable-pressure calorimeters A, B and C. Calorimeters A and B operate between atmospheric pressure and 0.3 GPa and use Bridgman thermocouples as thermal sensors. Calorimeter C operates up to 0.6 GPa and uses Peltier modules as thermal sensors. In calorimeter A, heating ramps within the temperature range from room temperature to 473 K were performed at 2 K min^{-1} using a resistive heater and cooling ramps were performed on average at -1 K min^{-1} with an air stream system. In calorimeters B and C, the temperature is controlled by a thermal jacket connected to an external thermal bath (Lauda Proline 1290), within the range $200 - 393 \text{ K}$, with temperature rate on heating of $\sim 2 \text{ K min}^{-1}$ and on cooling of $\sim -2 \text{ K min}^{-1}$. The sample was mixed in powder form with an inert fluid (Galden Bioblock Scientist) to remove air and encapsulated inside tin capsules that were attached to the thermal sensors. The pressure transmitting fluid was DW-Term M90.200.02

(Huber) and the pressure was measured using a high-pressure transducer Model HP from Honeywell (0.5% accuracy).

Supporting Information

Supporting Information is available from the Wiley Online Library or from the author.

Conflict of Interest

The authors declare no conflict of interest.

Acknowledgements

This work was supported by the MINECO project FIS2017-82625-P, the DGU project 2017SGR-42. J. Li would like to thank China Scholarship Council (CSC) and Queen Mary joint scholarship for his stay in U.K. A. E. Phillips and R. Dixey thank EPSRC for funding (EP/S03577X/1).

References

- [1] P. Lloveras, J.-L. Tamarit, *MRS Energy Sustain.* **2021**, *8* 3.
- [2] A. Kitanovski, *Adv. Energy Mater.* **2020**, *10* 1903741.
- [3] B. Li, Y. Kawakita, S. Ohira-Kawamura, T. Sugahara, H. Wang, J. Wang, Y. Chen, S. I. Kawaguchi, S. Kawaguchi, K. Ohara, K. Li, D. Yu, R. Mole, T. Hattori, T. Kikuchi, S.-I. Yano, Z. Zhang, Z. Zhang, W. Ren, S. Lin, O. Sakata, K. Nakajima, Z. Zhang, *Nature* **2019**, *567* 506.
- [4] P. Lloveras, A. Aznar, M. Barrio, P. Negrier, C. Popescu, A. Planes, L. Mañosa, E. Stern-Taulats, A. Avramenko, N. D. Mathur, X. Moya, J.-L. Tamarit, *Nat. Commun.* **2019**, *10* 1803.
- [5] J. M. Bermúdez-García, M. Sánchez-Andújar, S. Castro-García, J. López-Beceiro, R. Artiaga, M. A. Senarís-Rodríguez, *Nat. Commun.* **2017**, *8* 15715.
- [6] M. Szafranski, W.-J. Wei, Z.-M. Wang, W. Li, A. Katrusiak, *APL Mater.* **2018**, *6* 100701.
- [7] M. Romanini, Y. Wang, K. Gürpınar, G. Ornelas, P. Lloveras, Y. Zhang, W. Zheng, M. Barrio, A. Aznar, A. Gràcia-Condal, B. Emre, O. Atakol, C. Popescu, H. Zhang, Y. Long, L. Balicas, J. Lluís Tamarit, A. Planes, M. Shatruk, L. Mañosa, *Adv. Mater.* **2021**, *33* 2008076.
- [8] W. Li, Z. Wang, F. Deschler, S. Gao, R. H. Friend, A. K. Cheetham, *Nat. Rev. Materials* **2017**, *2* 16099.
- [9] V. Busico, C. Carfagna, V. Salerno, M. Vacatello, F. Fittipaldi, *Sol. Energy* **1980**, *24* 575.
- [10] D. Benson, R. Burrows, J. Webb, *Sol. Energy Mater.* **1986**, *13* 133.
- [11] T. Nakajima, H. Yamauchi, T. Goto, M. Yoshizawa, T. Suzuki, T. Fujimura, *J. Magn. Magn. Mater.* **1983**, *31-34* 1189.
- [12] R. Willett, E. Riedel, *Chem. Phys.* **1975**, *8* 112.
- [13] H. van Kempen, F. H. Mischgofsky, P. Wyder, *Phys. Rev. B* **1977**, *15* 4386.
- [14] K. Lee, C. Lee, *Solid State Commun.* **2003**, *126* 343.
- [15] B. Zhou, D. Yan, *Angew. Chem. Int. Ed.* **2019**, *58* 15128.
- [16] R. Gao, M. S. Kodaimati, D. Yan, *Chem. Soc. Rev.* **2021**, *50* 5564.
- [17] Y. Qin, Z. Lv, S. Chen, W. Li, X. Wu, L. Ye, N. Li, P. Lu, *J. Phys. Chem. C* **2019**, *123* 22491.
- [18] D. B. Mitzi, *J. Chem. Soc., Dalton Trans.* **2001**, 1–12.

- [19] L. Mao, C. C. Stoumpos, M. G. Kanatzidis, *J. Am. Chem. Soc.* **2019**, *141* 1171.
- [20] R. Blinc, M. Burgar, B. Lozzar, J. Seliger, J. Slak, V. Rutar, H. Arend, R. Kind, *J. Chem. Phys.* **1977**, *66* 278.
- [21] W.-W. Zhong, Y.-Y. Di, Y.-X. Kong, D.-F. Lu, J.-M. Dou, *J. Chem. Thermodyn.* **2014**, *72* 100.
- [22] G. F. Needham, R. D. Willett, H. F. Franzen, *J. Phys. Chem.* **1984**, *88* 674.
- [23] K. J. Schenk, G. Chapuis, *J. Phys. Chem.* **1988**, *92* 7141.
- [24] R. Kind, S. Plesko, H. Arend, R. Blinc, B. Zeks, J. Seliger, B. Lozar, J. Slak, A. Levstik, C. Filipic, V. Zagar, G. Lahajnar, F. Milia, G. Chapuis, *J. Chem. Phys.* **1979**, *71* 2118.
- [25] H. M. Rietveld, *J. Appl. Crystallogr.* **1969**, *2* 65.
- [26] A. A. Coelho, *J. Appl. Crystallogr.* **2018**, *51* 210.
- [27] M. R. Ciajolo, P. Corradini, V. Pavone, *Gazz. Chim. Ital.* **1976**, *106* 807.
- [28] M. Vacatello, P. Corradini, *Gazz. Chim. Ital.* **1973**, *103* 1027.
- [29] R. F. Schaufele, T. Shimanouchi, *J. Chem. Phys.* **1967**, *47* 3605.
- [30] W. L. Peticolas, G. W. Hibler, J. L. Lippert, A. Peterlin, H. Olf, *Appl. Phys. Lett.* **1971**, *18* 87.
- [31] M. Soutzidou, A. J. Masters, K. Viras, C. Booth, *Phys. Chem. Chem. Phys.* **1999**, *1* 415.
- [32] J. R. Scherer, R. G. Snyder, *J. Chem. Phys.* **1980**, *72* 5798.
- [33] L. Ricard, R. Cavagnat, M. Rey-Lafon, *J. Phys. Chem.* **1985**, *89* 4887.
- [34] H. L. Casal, D. G. Cameron, H. H. Mantsch, *J. Phys. Chem.* **1985**, *89* 5557.
- [35] Y. Abid, M. Kamoun, A. Daoud, F. Romain, *J. Raman Spectrosc.* **1990**, *21* 709.
- [36] F. Guillaume, G. Coddens, A. Dianoux, W. Petry, M. Rey-Lafon, C. Sourisseau, *Mol. Phys.* **1989**, *67* 665.
- [37] J. Li, D. Dunstan, X. Lou, A. Planes, L. Mañosa, M. Barrio, J.-L. Tamarit, P. Lloveras, *J. Mater. Chem. A* **2020**, *8* 20354.
- [38] E. Brück, H. Yibole, L. Zhang, *Philos. Trans. A Math. Phys. Eng. Sci.* **2016**, *374* 20150303.
- [39] L. Mañosa, A. Planes, *Appl. Phys. Lett.* **2020**, *116* 050501.
- [40] A. Aznar, P. Negrier, A. Planes, L. Mañosa, E. Stern-Taulats, X. Moya, M. Barrio, J.-L. Tamarit, P. Lloveras, *Appl. Mater. Today* **2021**, *23* 101023.

Colossal reversible barocaloric effects in layered hybrid perovskite (C₁₀H₂₁NH₃)₂MnCl₄ under low pressure near room temperature

Junning Li* María Barrio David J. Dunstan Richard Dixey Xiaojie Lou Josep-Lluís Tamarit Anthony E. Phillips Pol Lloveras*

Junning Li

Prof. David J. Dunstan

Dr. Richard Dixey

Dr. Anthony E. Phillips

School of Physics and Astronomy, Queen Mary University of London, London E1 4NS, United Kingdom

junning.li@qmul.ac.uk

Prof. Xiaojie Lou

Frontier Institute of Science and Technology, State Key Laboratory for Mechanical Behavior of Materials, Xi'an Jiaotong University, Xi'an 710049, China

Dr. María Barrio

Prof. Josep Lluís Tamarit

Dr. Pol Lloveras

Grup de Caracterizació de Materials, Departament de Física, EEBE and Barcelona Research Center in Multiscale Science and Engineering, Universitat Politècnica de Catalunya, Eduard Maristany, 10-14, 08019 Barcelona, Catalonia. pol.lloveras@upc.edu

Keywords: *Barocaloric effects, hybrid layered perovskites, calorimetry, phase diagram, Raman scattering*

We report barocaloric effects in a layered hybrid organic-inorganic compound, (C₁₀H₂₁NH₃)₂MnCl₄, that are reversible and colossal under pressure changes below 0.1 GPa. This barocaloric performance originates in a phase transition characterized by different features: A strong disordering of the organic chains, a very large volume change, a very large sensitivity of the transition temperature to pressure and a small hysteresis. Our obtained values are unprecedented among solid-state cooling materials at such low pressure changes and demonstrate that colossal effects can be obtained in compounds other than plastic crystals. The temperature-pressure phase diagram displays a triple point indicating enantiotropy at high pressure.

1 Introduction

In recent years, research on caloric effects induced by changes in applied hydrostatic pressure has experienced a significant growth [1], boosted by the urgent need of replacing hydrofluorocarbon-based devices that currently cause around ~8% of global greenhouse emissions [2]. A milestone has recently been achieved by the discovery of colossal barocaloric (BC) effects in plastic crystals [3, 4]. While these materials seem to represent an upper limit for the isothermal entropy changes, there is still room for improvement in terms of reducing the required pressure changes to obtain reversible barocaloric effects useful for real devices. Other systems such as hybrid organic-inorganic perovskites (HOIPs) [5, 6] and spin-crossover compounds [7] have revealed large reversible adiabatic temperature changes at moderate pressures along with giant isothermal entropy changes within large temperature spans, yielding excellent performance as BC agents thanks to phase transitions with small hysteresis and extreme sensitivity to pressure.

The extraordinary chemical flexibility in HOIPs allows a diversity of combinations that can be explored to tune their properties, seek optimal operational regimes and maximize performance. Indeed, HOIPs have raised great expectations in diverse areas of materials science due to their multifunctional properties, as used in photovoltaic technologies and optoelectronics [8]. Within such rich compositional and structural variety, an HOIP subfamily with the chemical formula (C_nH_{2n+1}NH₃)₂MCl₄ ($n = 1, 2, 3, \dots$), with M being a divalent metal, attracted particular interest in the 1970's [9] as phase change materials for thermal energy storage applications. As in the case of plastic crystals [10], this functionality emerges due to the occurrence of highly energetic, fully reversible first-order phase transitions with suitable transition temperatures. This feature, along with a large transition volume change, suggests that these com-

1
2 pounds could be very suitable as barocaloric agents, as plastic crystals have already shown. Compounds
3 with $M = \text{Mn, Fe}$ (and other very similar compounds), awakened further interest due to their low-dimensional
4 magnetic properties [11, 12, 13, 14] whereas other layered HOIPs are being investigated for photoluminis-
5 cence properties [15, 16, 17].

6
7 As in plastic crystals, the huge latent heat originates in the dynamic structural disorder released across
8 the transition. However, in contrast to the orientational disorder facilitated globular or small molecules
9 in plastic crystals, $(\text{C}_n\text{H}_{2n+1}\text{NH}_3)_2\text{MCl}_4$ compounds exhibit more complex structure and dynamical dis-
10 order. In particular, their structure has a 2-dimensional layered symmetry similar to lipid bilayers, dis-
11 playing a perovskite-like structure of reduced dimensionality with MCl_6 octahedra sharing their corners
12 only between neighbors in the (*ab*) planes. Between these planes there are two chains of alkylammonium
13 $\text{C}_n\text{H}_{2n+1}\text{NH}_3^+$ cations arranged along the *c* direction, whose length prevents the 3D corner-sharing along
14 this axis between octahedra belonging to different layers, as it does occur in true perovskites [18, 19].
15 These chains are linked at the ammonium end to the inorganic octahedra by electrostatic interactions
16 and hydrogen bonds. The organic chain tails facing each other are stabilized by their van der Waals in-
17 teractions [20, 21].

18
19 Often, these compounds show rich polymorphism already at atmospheric pressure, typically displaying
20 a sequence of two (sometimes more) transitions, one being significantly more energetic [9, 22, 23]. At
21 this major transition, while the organic chain remains ionically bonded to the inorganic part [24], some
22 gauche conformations arise in the alkyl bonds, which show dynamic mobility along the chain. This so-
23 called chain-melting process is at the origin of the huge entropy changes at the transition. The emer-
24 gence of the gauche conformations causes the chains to shorten. However, this is more than compensated
25 by the increase of the distance between the ends of the facing chains, leading to a significant positive net
26 volume change. The minor transition is order-disorder, where the disorder was concluded to consist of
27 the rigid chains rotating around the longitudinal chain axis between two equivalent orientations sepa-
28 rated by 90° , and with neighboring chains rotating in opposite directions. While not as enormous as the
29 major transition entropy change, the entropy change at the minor transition is still giant. The sequence
30 of these transitions is not unique; it may vary from one composition to another. The transition tempera-
31 tures increase with increasing *n*, which is consistent with the enhancement of the stability regime of the
32 ordered phase with the increasing chain length, that will be more difficult to destabilize. From $n = 9$
33 to $n = 17$ the transition temperature varies from 287 K to 373 K, thus offering a range of compositions
34 with caloric effects near room temperature.

35
36 Here we choose the compound $(\text{C}_{10}\text{H}_{21}\text{NH}_3)_2\text{MnCl}_4$ [$n = 10$, 10-bis(alkylammonium) tetrachloroman-
37 ganate(II), C_{10}Mn for short] because in this material the disorder fully develops across a single phase
38 transition and near room temperature and therefore exhibits a larger transition entropy change than
39 compounds with larger *n* values. Using pressure-dependent calorimetry and X-ray diffraction, we demon-
40 strate not only that colossal barocaloric effects can be obtained in compounds other than plastic crys-
41 tals, such as this layered HOIP family, but also that an improved BC performance can be obtained at
42 lower pressure than those reported so far in plastic crystals, due to a very small hysteresis and a very
43 large sensitivity of the transition temperature to pressure. Raman scattering experiments explore changes
44 in structure and dynamics across the transition.

45 2 Results and discussion

46 2.1 Structural and thermodynamic properties at atmospheric pressure

47
48 The structure of C_{10}Mn was characterized using X-ray powder diffraction (XRDP) measurements at at-
49 mospheric pressure and at temperatures around its solid-to-solid first-order phase transition. The diffrac-
50 tion patterns of the low-temperature phase at 295 K and of the high-temperature phase at 330 K were
51 refined by means of a Rietveld refinement procedure [25] using TOPAS-Academic v.7 [26]. At low tem-
52 peratures, a $P2_1/a$ structure (cif number: CCDC 2096682) was obtained, consistent with that reported
53
54
55
56
57

in Ref. [27], and in disagreement with the orthorhombic structure reported in Ref. [21]. For the high-temperature phase, which was previously undetermined, a $C2/m$ structure was obtained (cif number: CCDC 2096683). From these refinements, pattern matching of the temperature dependent XRDP patterns was performed, to obtain the unit cell volume as a function of temperature $V(T)$ (see Fig. 1a). This revealed a very large increase in volume at the endothermic transition of $\Delta V_t/V_{II} \sim 7\%$. A thorough explanation of the refinement details, the crystallographic structures of the unit cell in the two phases and the dependence of the patterns and the lattice parameters on temperature can be found in the Supplementary Material.

Isobaric temperature-dependent calorimetry at atmospheric pressure yielded positive and negative peaks in $dQ/|dT|$ associated with endothermic and exothermic first-order phase transitions, respectively (see Figure 1b). The maxima of the peaks were obtained at $T_{II \rightarrow I} = 312 \pm 1$ and $T_{I \rightarrow II} = 303 \pm 1$, whereas the onsets of the peaks at $T_{II \rightarrow I} = 309 \pm 1$ K and $T_{I \rightarrow II} = 306 \pm 1$ K. This shows a hysteresis of ~ 9 K as defined from the peak maxima, and ~ 3 K as defined from the peak onsets, which are both small. Integration over temperature of $dQ/|dT|$ and $(1/T)dQ/|dT|$ after baseline subtraction yielded transition enthalpy changes $\Delta H_{II \rightarrow I} = 76 \pm 4$ J g $^{-1}$ and $\Delta H_{I \rightarrow II} = 79 \pm 4$ J g $^{-1}$ and transition entropy changes $\Delta S_{II \rightarrow I} = 241 \pm 12$ J K $^{-1}$ kg $^{-1}$ and $\Delta S_{I \rightarrow II} = 261 \pm 13$ J K $^{-1}$ kg $^{-1}$, in very good agreement with the literature [27, 28]. The integrated curve for ΔS_t was used with the temperature-dependent heat capacity C_p obtained from modulated calorimetry (see Fig. 1c) to calculate the temperature-dependent entropy with respect to a reference temperature $T_0 = 213$ K (chosen arbitrarily below the transition) as $S(T, p_{\text{atm}}) - S(T_0, p_{\text{atm}}) = \int_{T_0}^T \frac{1}{T} (C_p + dQ/dT) dT$ (see Fig. 1d).

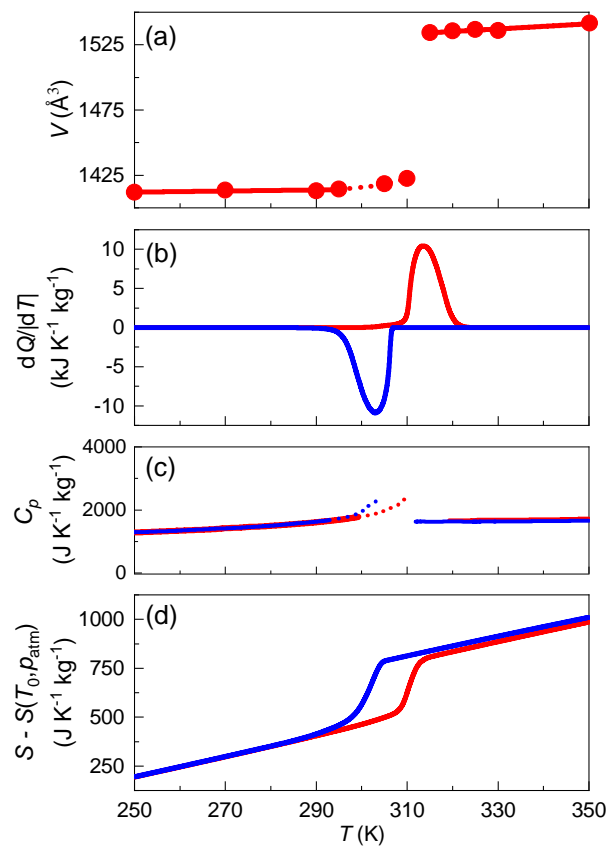


Figure 1: (a) Unit cell volume, (b) heat flow in temperature, (c) specific heat and (d) isobaric entropy as a function of temperature at atmospheric pressure. Red and blue curves correspond to data obtained on heating and on cooling, respectively.

To understand the origin of such large entropy changes at the transition, we investigated the molecular disordering process by temperature-dependent Raman scattering in both low and high wavenumbers. Previous Raman studies on organic chains have described a peak at low frequency as corresponding to

an accordion-like longitudinal acoustic mode (LAM) [29, 30, 31]. In our measurements, such a peak is obtained in the low temperature phase near 235 cm^{-1} (see Figure 2a). In particular, this is higher than the value for all-trans (T) chain (209 cm^{-1}) or for chains of the same length engaged in hydrogen bonds, such as n-decylamine (213 cm^{-1}) or decylammonium chloride (217 cm^{-1}) [32], and corresponds to a conformational effect and the existence of a gauche (G) conformation near the NH_3 polar head. In Fig. 2b, the characteristic bands of the trans planar chains are observed at 1065, 1109, 1146 and 1174 cm^{-1} . This indicates that the most intense bands in the Raman spectrum of the long alkyl chains correspond to the limiting $k = 0$ modes of an infinite chain [33]. Figures 2c and 2d show the characteristic bands of the C-H twisting (1300 cm^{-1}), bending ($1420\text{-}1480 \text{ cm}^{-1}$) and stretching ($2830\text{-}3000 \text{ cm}^{-1}$) mode. It is worth noting that the scattering wing on the 2846 cm^{-1} line is due to intermolecular forces [33]. Moreover, the Mn-Cl stretching mode band can be found at 186 and 236 cm^{-1} (overlapped with LAM at 235 cm^{-1}) and wavenumbers 300, 1040 and 1080 cm^{-1} correspond to the NH_3 torsional band (overlapped with the trans bond stretching at 300 cm^{-1}) [34, 35]. Overall, the low-temperature study of these spectral regions indicates a typical ordered state of the low-temperature phase and gives further evidence for the existence of inter- and intramolecular coupling in an almost completely extended chain. In the high-temperature phase, the Raman spectra indicate the emergence of disorder. Firstly, the LAM mode and the limiting $k = 0$ mode bands disappear and only a broad and weak band is observed near 247 cm^{-1} , which means the conformation of the long trans planar chains is changed. Further evidence of appearing of the gauche bond structure can be found in the decrease of the 1465 cm^{-1} shoulder, which is due to intramolecular coupling of trans structures [33, 35]. In order to fully understand the structure of the organic part, we schematically show the probable conformation of the decylammonium chain as reported in the literature from infrared spectra [27] and incoherent neutron scattering [36]. In Figures 2e and 2f we can see that the conformation for low temperature is T-G-T-T-T-T-T-T while the high temperature becomes T-T-T-G-T-G'-T. As discussed previously, it is believed that the reorientation of the whole chain and the disorder of the hydrocarbon parts comes from the increase of the G and G' conformation which is regarded as conformational disorder and contributes a large latent heat in the order-disorder first-order phase transition. Furthermore, the C-H stretching mode bands at 2870, 2883 and 2930 cm^{-1} merge into a broad scattering peak, indicating that the intermolecular forces were greatly changed. Finally, the Mn-Cl stretching mode bands become weak and broad at high temperature with the disappearing of the NH_3 torsional mode band. This means a dramatic change for the layer, which is consistent with the increase of the c -axis length from the XRD data (see Supplementary Figure S4).

2.2 Thermodynamic properties at high pressure

Isobaric temperature-dependent calorimetry performed at selected pressures (see Figure 3a and Supplementary Figure S5) below 0.1 GPa reveals single peaks associated with the $\text{II} \leftrightarrow \text{I}$ transition, that shift strongly to higher temperatures with increasing pressure (see Figures 3b-d). This shift can be fitted by slightly convex second-order polynomials, yielding $\frac{dT_{\text{II} \rightarrow \text{I}}}{dp} = 250 \pm 6 \text{ K GPa}^{-1}$ and $\frac{dT_{\text{I} \rightarrow \text{II}}}{dp} = 280 \pm 20 \text{ K GPa}^{-1}$ for the endothermic and exothermic transitions, respectively, at atmospheric pressure. Above 0.15 GPa, the endothermic calorimetric signals clearly exhibit two consecutive peaks which indicate the appearance of a new phase (III) between the two peaks. The larger peak corresponds to the transition $\text{II} \rightarrow \text{III}$ and is followed by the smaller peak corresponding to the $\text{III} \rightarrow \text{I}$. The exothermic transitions show the peak splitting at lower pressures. Two possible causes are, (i) the occurrence of transitions between equilibrium phases, I-III-II , but with different hysteresis (i.e. a larger thermal hysteresis of the transition $\text{III} \rightarrow \text{II}$ than that of the transition $\text{I} \rightarrow \text{II}$), for which the peak splitting can be more easily identified in exothermic peaks than in endothermic peaks because in the latter the overlap of the very close peaks prevents distinguishing them; (ii) the occurrence of a metastable phase transition from the equilibrium phase I to the metastable phase III at temperatures and pressures below the triple point in equilibrium, followed by a phase transition from the metastable phase III to the stable phase II. Or a combination of (i) and (ii) is possible. The striking similarity between the $\frac{dT}{dp}$ values of the different coexistence lines ($\frac{dT_{\text{II} \rightarrow \text{III}}}{dp} = 180 \pm 1 \text{ K GPa}^{-1}$, $\frac{dT_{\text{III} \rightarrow \text{II}}}{dp} = 161 \pm 2 \text{ K GPa}^{-1}$, $\frac{dT_{\text{III} \rightarrow \text{I}}}{dp} = 170 \pm 2 \text{ K GPa}^{-1}$, $\frac{dT_{\text{I} \rightarrow \text{III}}}{dp} = 160 \pm 3 \text{ K GPa}^{-1}$)

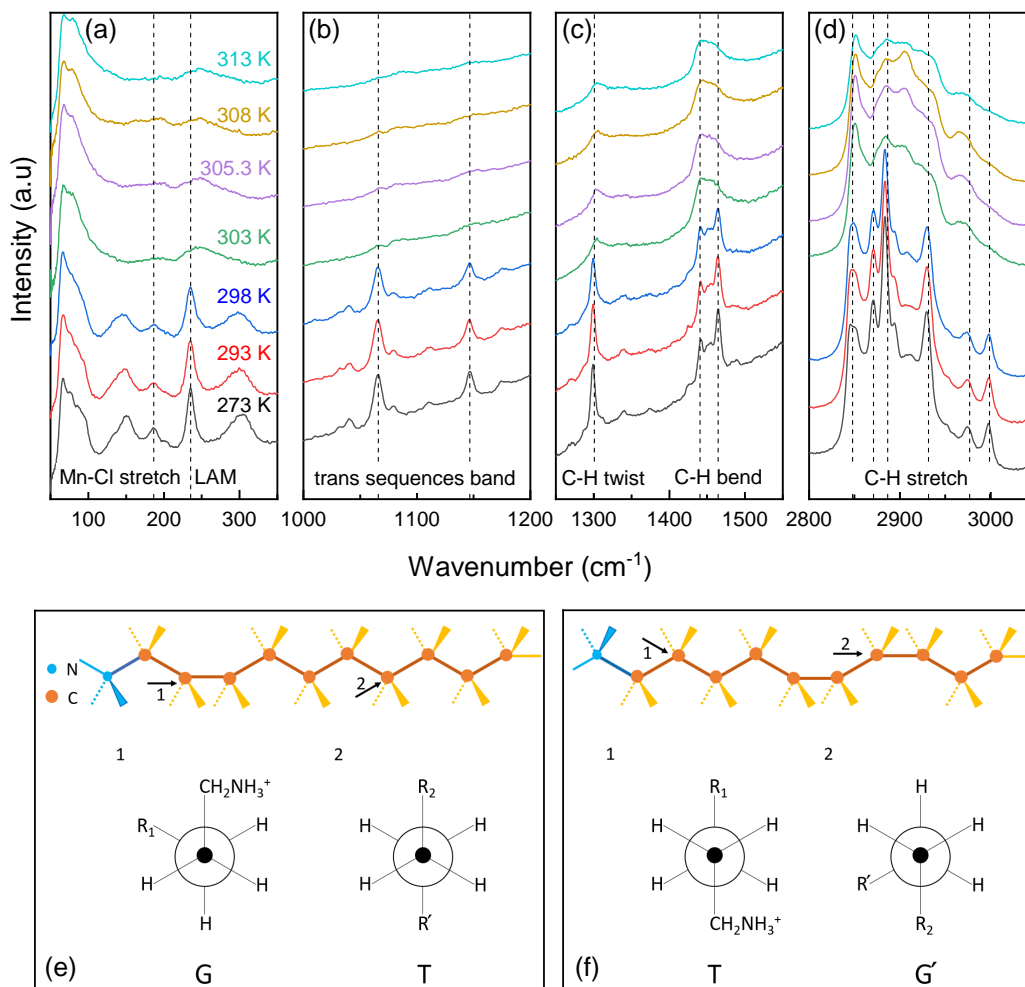


Figure 2: (a-d) Temperature dependence of the Raman spectrum of $(C_{10}H_{21}NH_3)_2MnCl_4$ at different wave number intervals. (e,f) Schematic diagram for the probable conformation of the decylammonium chain under low and high temperature respectively, along with Newman projections for trans (T) and gauche (G) conformations corresponding to the positions indicated by numbers 1 and 2. R_1 stands for $-CH_2-CH_2-CH_2-CH_2-CH_2-CH_2-CH_3$. R_2 stands for $-CH_2-CH_2-CH_2-CH_2-CH_2-CH_2-NH_3^+$. R' stands for $-CH_2-CH_3$.

GPa⁻¹) makes it even more difficult to determine the actual cause. Moreover, this behavior prevents an accurate determination of the coordinates of the triple point where phases I, II and III coexist in equilibrium, (T_{tp}, p_{tp}) , as cause (i) would lead the triple point to be at (~ 330 K, ~ 0.12 GPa) whereas cause (ii) would lead the triple point to be closer to (~ 337 K, ~ 0.14 GPa). On the other hand, notice that at the highest applied pressure $p = 0.36$ GPa the exothermic peaks are observed in the inverse order, with first the larger peak followed by the smaller peak. This behavior can only be explained if part of the material undergoes a phase transition from stable phase I towards a metastable phase II, which on further cooling becomes stable, while the rest of the material undergoes the transition sequence between stable phases $I \rightarrow III \rightarrow II$.

Integration of the peaks in $(1/T)(dQ/|dT|)$ at different pressures reveals that the transition entropy change decays significantly with increasing pressure, at a rate of $\sim -1.1 \cdot 10^3$ J K⁻¹ kg⁻¹ GPa⁻¹ (see Figure 3e). Close to the triple point, we obtained $\Delta S_{II \rightarrow I}(p \sim 0.15$ GPa) = 144 ± 14 J K⁻¹ kg⁻¹, $\Delta S_{II \rightarrow III} = 102 \pm 10$ J K⁻¹ kg⁻¹ and $\Delta S_{III \rightarrow I} = 32 \pm 4$ J K⁻¹ kg⁻¹. For the exothermic transitions we obtained $\Delta S_{II \rightarrow I}(p \sim 0.15$ GPa) = 196 ± 20 J K⁻¹ kg⁻¹, $\Delta S_{II \rightarrow III} = 134 \pm 14$ J K⁻¹ kg⁻¹ and $\Delta S_{III \rightarrow I} = 60 \pm 6$ J K⁻¹ kg⁻¹. Notice that these values are consistent with the thermodynamic requirement at the triple point $\Delta S_{II \rightarrow I} \sim \Delta S_{II \rightarrow III} + \Delta S_{III \rightarrow I}$. By comparison with the transition sequence exhibited by other compounds

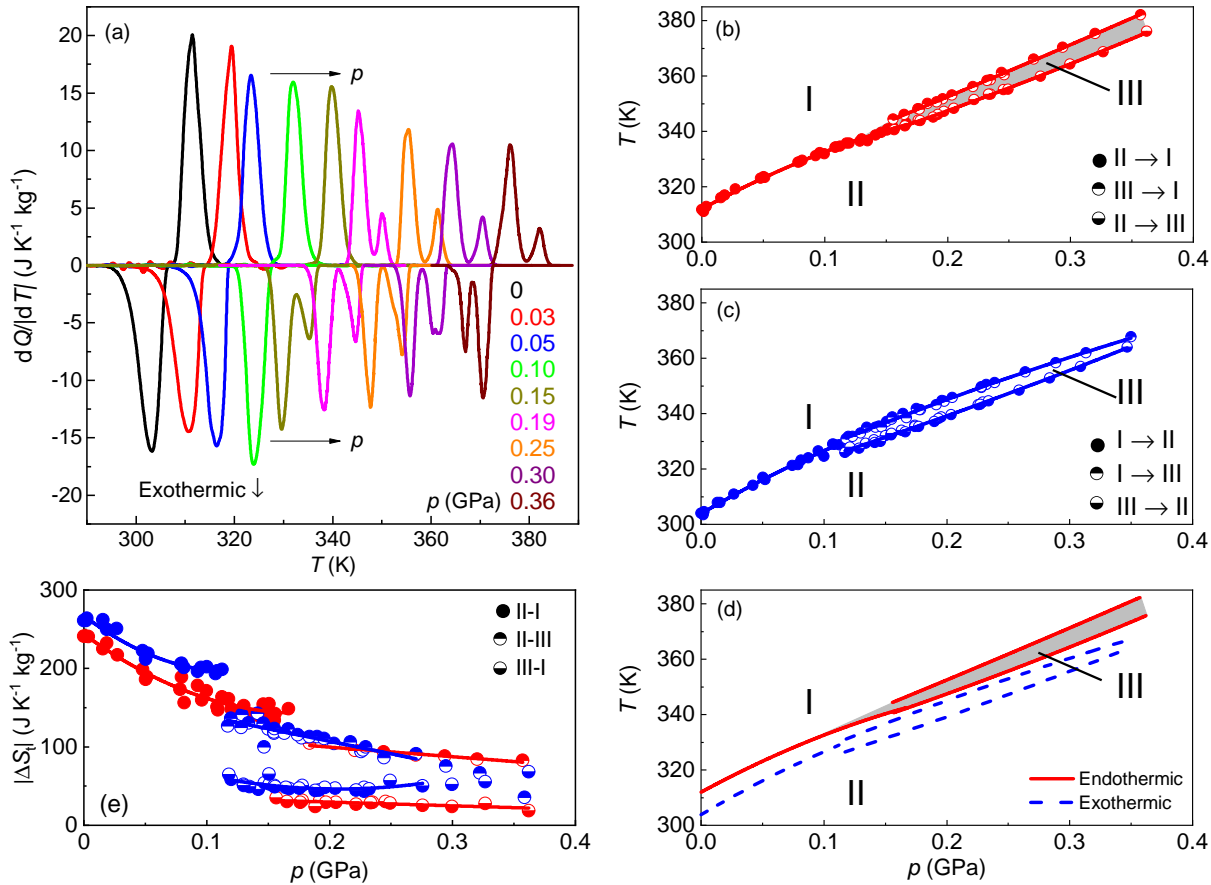


Figure 3: (a) Isobaric heat flow $dQ/|dT|$ as a function of temperature at different applied pressures on heating (positive peaks) and on cooling (negative peaks). (b-d) Transition temperatures as a function of pressure determined as the maximum of the peaks. For the sake of clarity, endothermic (b) and exothermic (c) data are shown separately. Panel (d) shows the fits for both endothermic and exothermic transitions. Shaded areas show the equilibrium region for phase III. (e) Transition entropy change as a function of the applied pressure, for the endothermic (red) and exothermic (blue) transitions. Filled symbols, top-half filled symbols and bottom-half filled symbols stand for $\text{II} \leftrightarrow \text{I}$, $\text{III} \leftrightarrow \text{I}$ and $\text{II} \leftrightarrow \text{III}$ transitions, respectively. Lines are fits to data.

of the same family at atmospheric pressure [9, 22, 23], and given that $\Delta S_{\text{II} \rightarrow \text{III}}$ is significantly larger than $\Delta S_{\text{III} \rightarrow \text{I}}$, we expect that above the triple point the $\text{II} \rightarrow \text{III}$ transition is the major transition involving the chain melting whereas the $\text{III} \rightarrow \text{I}$ transition corresponds to the minor transition of the order-disorder type. On the other hand, given the inverse transition order obtained on cooling in a very few cases, to avoid any inconsistency in the determination of $\Delta S_{\text{I} \rightarrow \text{III}}$ and $\Delta S_{\text{III} \rightarrow \text{II}}$, we have omitted the integration values at high pressure when performing the fits to the data displayed in Figure 3e and when determining the BC effects. Also, it is worth noticing that the joint integration of the two peaks shows a smooth and monotonic behavior regardless of the transition order (see Supplementary Figure S6). This strongly indicates that the transitions order does not affect the thermodynamic properties associated with the overall transition path $\text{I} \rightarrow \text{II}$.

2.3 Determination of entropy as a function of temperature and pressure

To calculate the barocaloric effect via the quasi-direct method, the isobaric entropy as a function of temperature and for different pressures, $S(T, p)$ was obtained with respect to a reference taken at temperature T_0 and atmospheric pressure. The procedure to obtain $S(T, p)$ consisted of integration of a TdS equation for an homogeneous system, extended to include a phase transition contribution, which can be expressed mathematically as:

$$S(T, p) = S(T_0, p_{\text{atm}}) - \int_{p_{\text{atm}}}^p \left(\frac{\partial V}{\partial T} \right)_p dp + \int_{T_0}^T \frac{1}{T'} \left(C_p(T', p) + \frac{dQ}{|dT'|} (T', p) \right) dT'. \quad (1)$$

At $T = T_0$, the integral over temperature vanishes and we obtained $S(T_0, p)$ through an isothermal path from $S(T_0, p_{\text{atm}})$ via the integral over pressure in Eq. 1, which was approximated to $\simeq \left(\frac{\partial V}{\partial T} \right)_{p_{\text{atm}}} p$. Above T_0 , $S(T, p)$ was calculated through the integral over temperature. There, $\frac{dQ}{|dT'|} (T', p)$ is the temperature- and pressure-dependent transition heat flow shown in Figure 4a and $C_p(T', p)$ accounts for the isobaric heat capacity (shown in Supplementary Figure S7). The temperature dependence of C_p in the transition temperature interval was estimated as a weighted average of the two phases I and II, i.e. $C_p(T', p) = (1 - x)C_p^{\text{II}}(T', p) + xC_p^{\text{I}}(T', p)$, where $x(T)$ is the fraction of the system in phase I and is computed using the normalized cumulative integral for the transition entropy change. The former expression is also used for pressures above the triple point, where the C_p of phase III is experimentally inaccessible. However, given the very narrow temperature range of stability of this phase, the error introduced in the entropy due to this approximation is expected to be insignificant.

The pressure dependence of C_p was evaluated from the temperature dependence of the volume by means of the thermodynamic relation $\left(\frac{\partial C_p}{\partial p} \right)_T = -T \left(\frac{\partial^2 V}{\partial T^2} \right)_p$. According to our data, $V(T)$ is approximately linear in phase II below ~ 295 K and in phase I in the measured interval (see red linear fit in Figure 1a), indicating that C_p is independent of pressure in these temperature intervals (red and blue lines in Figure 1c). Instead, $V(T)$ is nonlinear in the temperature interval (295 – 310) K (see dashed line in Figure 1a), indicating a pressure dependence C_p in this temperature interval (see dashed lines in Figure 1c). Moreover, as the transition temperature increases with pressure, these C_p features must be translated to higher temperatures with increasing pressure an amount $(dT/dp)(p - p_{\text{atm}})$. Calculated $C_p(T, p)$ curves are shown in Supplementary Figure S8. A very detailed explanation of the procedure for the construction of the $C_p(T, p)$ curves can be found in Ref. [37]. The resulting functions $S(T, p) - S(T_0, p_{\text{atm}})$ are shown in Figure 4(a,b) for selected pressures.

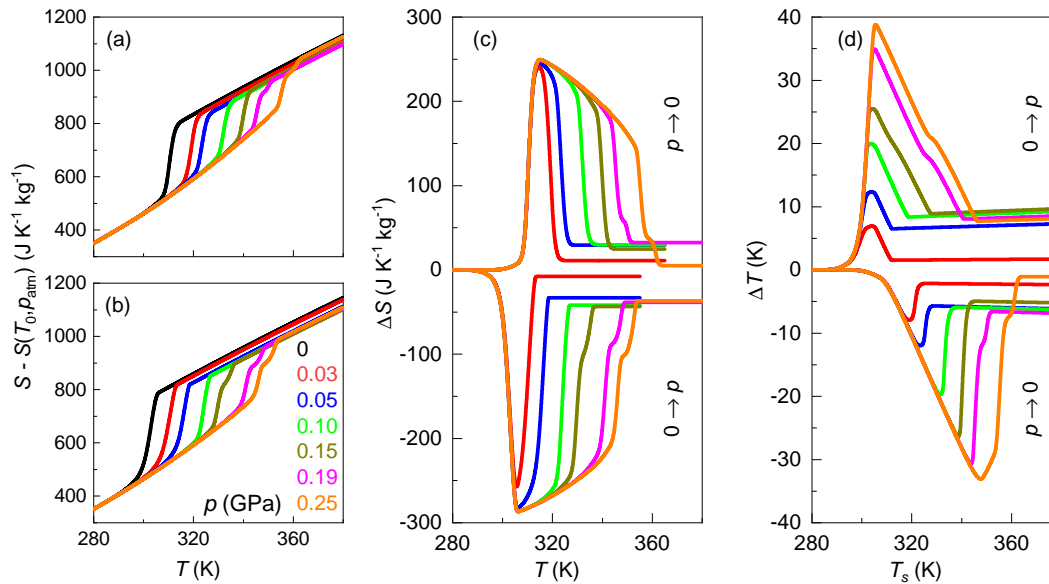


Figure 4: Isobaric entropy as a function of temperature for different values of applied pressure, on heating (a) and on cooling (b). (c) Isothermal entropy changes as a function of temperature and (d) adiabatic temperature changes as a function of the starting temperature, for different values of pressure changes on first compression and on first decompression.

2.4 Barocaloric effects and performance

BC effects were calculated from or to atmospheric pressure so that pressure changes will be approximated to $|\Delta p| \sim p$. For phase transitions with $dT/dp > 0$, transitions on decompression (compression) are endothermic (exothermic) and therefore BC effects, ΔS and ΔT , on first decompression (compression) must be computed from isobaric entropy functions on heating [$S_H(T; p)$] (cooling, [$S_C(T; p)$]), as displayed in Figure 4(c,d). More importantly, this feature entails that the reversible ΔT usable in cooling devices that work in sequential compression–decompression cycles, are given by $|\Delta T_{\text{rev}}(S; p_{\text{atm}} \leftrightarrow p)| = |T_C(S; p) - T_H(S; p_{\text{atm}})|$. In turn, ΔS_{rev} can be determined as the overlapping between $\Delta S(T; p_{\text{atm}} \rightarrow p)$ and $\Delta S(T; p \rightarrow p_{\text{atm}})$. The obtained results (shown in Figure 5a,b) reveal reversible values for ΔS_{rev} that exceed $100 \text{ J K}^{-1} \text{ kg}^{-1}$ under pressure changes as low as 0.03 GPa, and are colossal ($\sim 230 \text{ J K}^{-1} \text{ kg}^{-1}$) under $p \sim 0.05 \text{ GPa}$. Under $p \sim 0.1 \text{ GPa}$, we obtain colossal BC effects of $\Delta S_{\text{rev}} \sim 250 \text{ J K}^{-1} \text{ kg}^{-1}$ and $\Delta T_{\text{rev}} \sim 12 \text{ K}$, with a refrigerant capacity $RC \equiv \int \Delta S_{\text{rev}} dT \sim 3.5 \text{ kJ kg}^{-1}$ (see Figure 5c). Joint values for ΔS_{rev} and ΔT_{rev} are plotted in Figure 6a for different applied pressure changes as a function of temperature. The temperature span where these effects occur near room temperature are plotted as a function of the applied pressure change p in Figure 6b and 6c for ΔS_{rev} and ΔT_{rev} , respectively. For instance, at $p \sim 0.1 \text{ GPa}$, at least $\Delta S \sim 100 \text{ J K}^{-1} \text{ kg}^{-1}$ are obtained within an interval of $\sim 13 \text{ K}$.

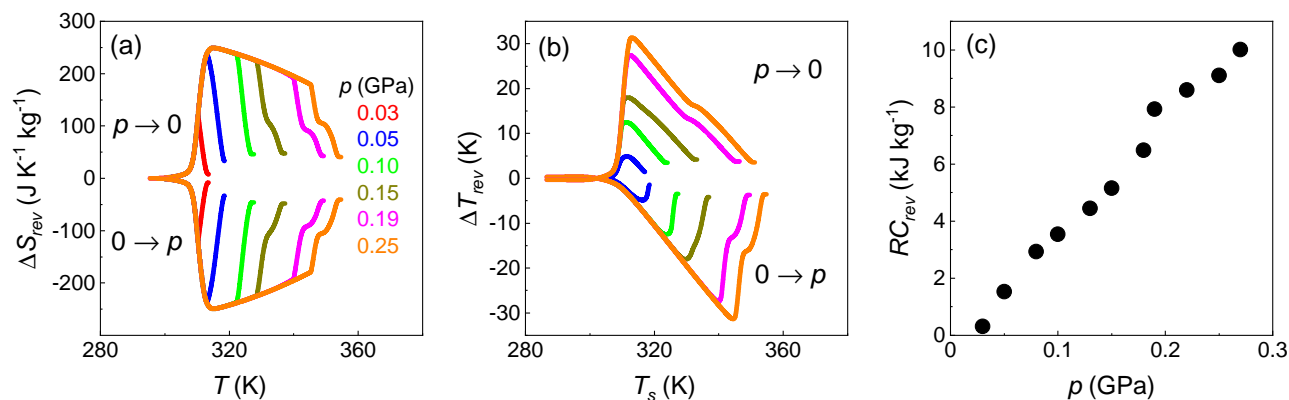


Figure 5: Reversible (a) isothermal entropy changes and (b) adiabatic temperature changes upon application and removal of pressure changes from or to atmospheric pressure, as a function of temperature. (c) Reversible refrigerant capacity as a function of pressure change.

Finally, we calculate the Coefficient of Refrigerant Performance (CRP) [38, 39] for comparison with other BC materials (see Figure 7). The set of values for this compound are comparable to or better than the best reversible BC effects reported so far (e.g. 1-Br-ada and 1-Cl-ada [1, 40]). Particularly interesting is the low pressure change for which these excellent values are obtained, which brings BC materials closer to real applications, such as solid-state cooling or heat pumping. Our study paves the way for finding colossal BC effects in compounds beyond plastic crystals, thus widening the range of suitable materials and stimulating the research in similar compounds. This is especially appealing in this family of compounds because material properties can be sensitively tuned to match desired features by changing the chain length and/or by chemical substitution of the cation.

3 Conclusions

In this work we have demonstrated colossal barocaloric effects in a hitherto unexplored material family, the hybrid organic-inorganic layered perovskites. In particular, $(\text{C}_{10}\text{H}_{21}\text{NH}_3)_2\text{MnCl}_4$ undergoes reversible isothermal entropy changes of $\sim 230 \text{ J K}^{-1} \text{ kg}^{-1}$ under low pressure changes of 0.05 GPa, and reversible adiabatic temperature changes of $\sim 10 \text{ K}$ under pressure changes of 0.08 GPa near room temperature, which are outstanding compared to other solid-state materials. The origin of this extremely good response is a very large increase in entropy and volume associated with the melting of the organic chain

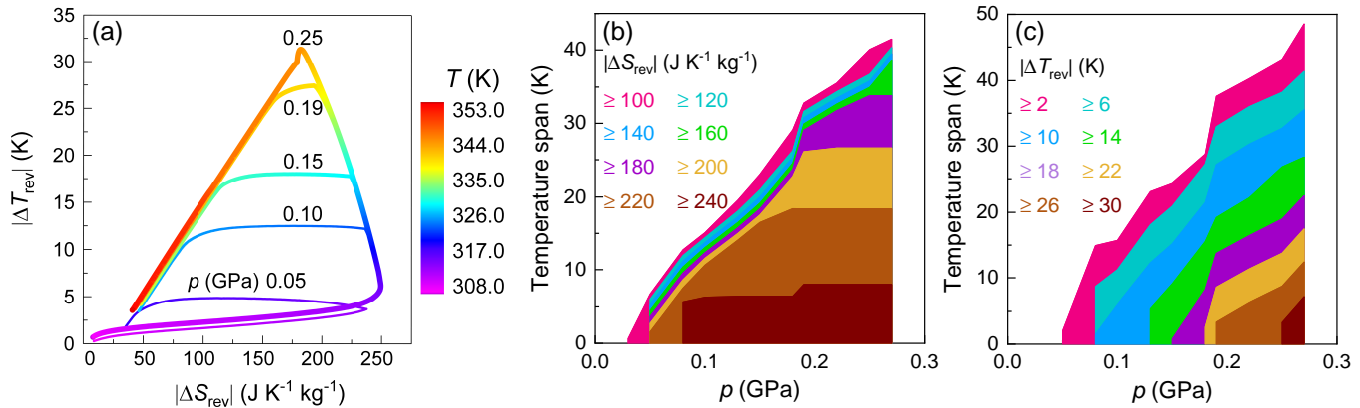


Figure 6: (a) Reversible adiabatic temperature changes and isothermal entropy changes that can be obtained at different applied pressures changes, occurring at temperatures indicated by the color code. Temperature span where a range of (b) isothermal entropy changes and (c) adiabatic temperature changes take place, as a function of the required pressure change.

across a sharp and low-hysteresis first-order solid-solid phase transition. This compound not only widens the horizons for colossal barocaloric materials to include other compounds beyond the canonical plastic crystals but it also expands the limits for the barocaloric performance in solid-state materials. Our results suggest that this compound is among the best candidates to be exploited as a barocaloric agent in pressure-driven solid-state cooling.

4 Experimental Section

Preparation of the sample:

The $(\text{C}_{10}\text{H}_{21}\text{NH}_3)_2\text{MnCl}_4$ sample was prepared by using a two-step reaction method. Manganese(II) chloride tetrahydrate ($\text{MnCl}_2 \cdot 4\text{H}_2\text{O}$, 99%, Sigma Aldrich) was added into hydrochloric acid (HCl, 36.5 to 38.0%, Baker Analyzed) with magnetic stirring until $\text{MnCl}_2 \cdot 4\text{H}_2\text{O}$ was fully dissolved. Then, n-decylamine ($\text{C}_{10}\text{H}_{21}\text{NH}_2$, 99%, ACROS Organics) was added into this mixed solution with magnetic stirring for 3 hours. Then, $(\text{C}_{10}\text{H}_{21}\text{NH}_3)_2\text{MnCl}_4$ powder was obtained by precipitation and washed with ethanol twice. The total yield of the compound is $\simeq 72\%$.

X-ray Diffraction:

X-ray diffraction patterns were obtained using two diffractometers: A Siemens D5000 X-ray Powder diffractometer using monochromatic $\text{Cu-K}_{\alpha 1}$ radiation was employed to check the purity of the synthesized samples because impurities have been reported to modify thermodynamic transition data [22]. An INEL diffractometer with $\text{Cu-K}_{\alpha 1} = 1.5406 \text{ \AA}$ radiation, a curved position-sensitive detector (CPS120), a 0.5-mm-diameter Lindemann capillary and a 700 series Oxford Cryostream Cooler to control the temperature were used to perform temperature-dependent high-resolution X-ray powder diffraction measurements at atmospheric pressure and different temperatures.

Raman Spectroscopy:

Raman spectra were obtained using an IK Series Raman spectroscopy system. A 532 nm He-Cd laser was used for excitation. A calibrated Linkam heating-cooling stage was utilized to control sample temperature, via a thermocouple attached to the sample holder.

Differential scanning calorimetry (DSC):

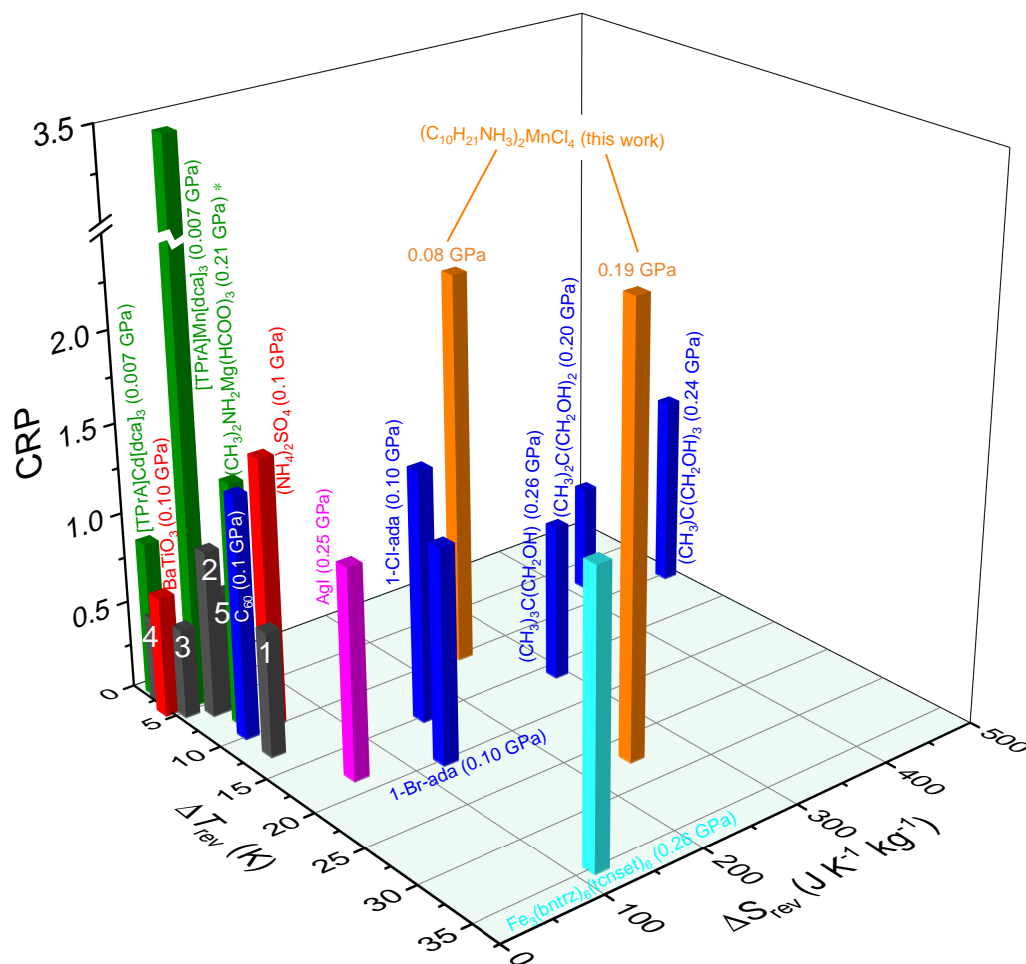


Figure 7: Coefficient of Refrigerant Performance, reversible adiabatic temperature changes and reversible isothermal entropy changes for different materials reported in literature [1]. Label 1 corresponds to MnCoGeB_{0.03}, 2 to Co₅₀Fe_{2.5}V_{31.5}Ga₁₆, 3 to Fe₄₉Rh₅₁, 4 to Ni_{35.5}Co_{14.5}Mn₃₅Ti₁₅ and 5 to MnNiSi_{0.61}FeCoGe_{0.39}. Color bars stand for different types of transitions: Black refer to ferromagnetic or metamagnetic systems, cyan to spin-crossover compounds, magenta to superionic conductors, red to ferroelectric inorganic salts, blue to plastic crystals, green to hybrid organic-inorganic perovskites and orange to the hybrid compound studied in this work. *The value of ΔT used for (CH₃)₂NH₂Mg(HCOO)₃ is irreversible.

DSC at atmospheric pressure was performed using a Q100 DSC from TA Instruments. A few mg were hermetically encapsulated into the Al capsule sample-holders. Heating and cooling ramps were performed at ± 2 K min⁻¹. Measurements of specific heat C_p were performed at atmospheric pressure in a commercial differential scanning calorimeter (DSC, TA Q2000), at 5 K min⁻¹, using ~ 5 mg samples of (C₁₀H₂₁NH₃)₂MnCl₄. The amplitude was 0.5 K and period was 60 s. The heating and cooling rate were 2 K min⁻¹.

High-Pressure differential thermal analysis (HP-DTA):

HP-DTA was performed using three different bespoke variable-pressure calorimeters A, B and C. Calorimeters A and B operate between atmospheric pressure and 0.3 GPa and use Bridgman thermocouples as thermal sensors. Calorimeter C operates up to 0.6 GPa and uses Peltier modules as thermal sensors.

In calorimeter A, heating ramps within the temperature range from room temperature to 473 K were performed at 2 K min⁻¹ using a resistive heater and cooling ramps were performed on average at -1 K min⁻¹ with an air stream system. In calorimeters B and C, the temperature is controlled by a thermal jacket connected to an external thermal bath (Lauda Proline 1290), within the range 200 – 393 K, with temperature rate on heating of ~ 2 K min⁻¹ and on cooling of ~ -2 K min⁻¹. The sample was mixed in powder form with an inert fluid (Galden Bioblock Scientist) to remove air and encapsulated inside tin capsules that were attached to the thermal sensors. The pressure transmitting fluid was DW-Term M90.200.02

(Huber) and the pressure was measured using a high-pressure transducer Model HP from Honeywell (0.5% accuracy).

Supporting Information

Supporting Information is available from the Wiley Online Library or from the author.

Conflict of Interest

The authors declare no conflict of interest.

Acknowledgements

This work was supported by the MINECO project FIS2017-82625-P, the DGU project 2017SGR-42. J. Li would like to thank China Scholarship Council (CSC) and Queen Mary joint scholarship for his stay in U.K. A. E. Phillips and R. Dixey thank EPSRC for funding (EP/S03577X/1).


References


- [1] P. Lloveras, J.-L. Tamarit, *MRS Energy Sustain.* **2021**, *8* 3 .
- [2] A. Kitanovski, *Adv. Energy Mater.* **2020**, *10* 1903741.
- [3] B. Li, Y. Kawakita, S. Ohira-Kawamura, T. Sugahara, H. Wang, J. Wang, Y. Chen, S. I. Kawaguchi, S. Kawaguchi, K. Ohara, K. Li, D. Yu, R. Mole, T. Hattori, T. Kikuchi, S.-I. Yano, Z. Zhang, Z. Zhang, W. Ren, S. Lin, O. Sakata, K. Nakajima, Z. Zhang, *Nature* **2019**, *567* 506.
- [4] P. Lloveras, A. Aznar, M. Barrio, P. Negrier, C. Popescu, A. Planes, L. Mañosa, E. Stern-Taulats, A. Avramenko, N. D. Mathur, X. Moya, J.-L. Tamarit, *Nat. Commun.* **2019**, *10* 1803.
- [5] J. M. Bermúdez-García, M. Sánchez-Andújar, S. Castro-García, J. López-Beceiro, R. Artiaga, M. A. Senarís-Rodríguez, *Nat. Commun.* **2017**, *8* 15715.
- [6] M. Szafranski, W.-J. Wei, Z.-M. Wang, W. Li, A. Katrusiak, *APL Mater.* **2018**, *6* 100701.
- [7] M. Romanini, Y. Wang, K. Gürpınar, G. Ornelas, P. Lloveras, Y. Zhang, W. Zheng, M. Barrio, A. Aznar, A. Gràcia-Condal, B. Emre, O. Atakol, C. Popescu, H. Zhang, Y. Long, L. Balicas, J. Lluís Tamarit, A. Planes, M. Shatruk, L. Mañosa, *Adv. Mater.* **2021**, *33* 2008076.
- [8] W. Li, Z. Wang, F. Deschler, S. Gao, R. H. Friend, A. K. Cheetham, *Nat. Rev. Materials* **2017**, *2* 16099.
- [9] V. Busico, C. Carfagna, V. Salerno, M. Vacatello, F. Fittipaldi, *Sol. Energy* **1980**, *24* 575 .
- [10] D. Benson, R. Burrows, J. Webb, *Sol. Energy Mater.* **1986**, *13* 133 .
- [11] T. Nakajima, H. Yamauchi, T. Goto, M. Yoshizawa, T. Suzuki, T. Fujimura, *J. Magn. Magn. Mater.* **1983**, *31-34* 1189.
- [12] R. Willett, E. Riedel, *Chem. Phys.* **1975**, *8* 112.
- [13] H. van Kempen, F. H. Mischgofsky, P. Wyder, *Phys. Rev. B* **1977**, *15* 4386.
- [14] K. Lee, C. Lee, *Solid State Commun.* **2003**, *126* 343.
- [15] B. Zhou, D. Yan, *Angew. Chem. Int. Ed.* **2019**, *58* 15128.
- [16] R. Gao, M. S. Kodaimati, D. Yan, *Chem. Soc. Rev.* **2021**, *50* 5564.
- [17] Y. Qin, Z. Lv, S. Chen, W. Li, X. Wu, L. Ye, N. Li, P. Lu, *J. Phys. Chem. C* **2019**, *123* 22491.
- [18] D. B. Mitzi, *J. Chem. Soc., Dalton Trans.* **2001**, 1–12.

- 1
2 [19] L. Mao, C. C. Stoumpos, M. G. Kanatzidis, *J. Am. Chem. Soc.* **2019**, *141* 1171.
3
4 [20] R. Blinc, M. Burgar, B. Lozzar, J. Seliger, J. Slak, V. Rutar, H. Arend, R. Kind, *J. Chem. Phys.*
5 **1977**, *66* 278.
6
7 [21] W.-W. Zhong, Y.-Y. Di, Y.-X. Kong, D.-F. Lu, J.-M. Dou, *J. Chem. Thermodyn.* **2014**, *72* 100.
8
9 [22] G. F. Needham, R. D. Willett, H. F. Franzen, *J. Phys. Chem.* **1984**, *88* 674.
10
11 [23] K. J. Schenk, G. Chapuis, *J. Phys. Chem.* **1988**, *92* 7141.
12
13 [24] R. Kind, S. Plesko, H. Arend, R. Blinc, B. Zeks, J. Seliger, B. Lozar, J. Slak, A. Levstik, C. Filipic,
14 V. Zagar, G. Lahajnar, F. Milia, G. Chapuis, *J. Chem. Phys.* **1979**, *71* 2118.
15
16 [25] H. M. Rietveld, *J. Appl. Crystallogr.* **1969**, *2* 65.
17
18 [26] A. A. Coelho, *J. Appl. Crystallogr.* **2018**, *51* 210.
19
20 [27] M. R. Ciajolo, P. Corradini, V. Pavone, *Gazz. Chim. Ital.* **1976**, *106* 807.
21
22 [28] M. Vacatello, P. Corradini, *Gazz. Chim. Ital.* **1973**, *103* 1027.
23
24 [29] R. F. Schaufele, T. Shimanouchi, *J. Chem. Phys.* **1967**, *47* 3605.
25
26 [30] W. L. Peticolas, G. W. Hibler, J. L. Lippert, A. Peterlin, H. Olf, *Appl. Phys. Lett.* **1971**, *18* 87.
27
28 [31] M. Soutzidou, A. J. Masters, K. Viras, C. Booth, *Phys. Chem. Chem. Phys.* **1999**, *1* 415.
29
30 [32] J. R. Scherer, R. G. Snyder, *J. Chem. Phys.* **1980**, *72* 5798.
31
32 [33] L. Ricard, R. Cavagnat, M. Rey-Lafon, *J. Phys. Chem.* **1985**, *89* 4887.
33
34 [34] H. L. Casal, D. G. Cameron, H. H. Mantsch, *J. Phys. Chem.* **1985**, *89* 5557.
35
36 [35] Y. Abid, M. Kamoun, A. Daoud, F. Romain, *J. Raman Spectrosc.* **1990**, *21* 709.
37
38 [36] F. Guillaume, G. Coddens, A. Dianoux, W. Petry, M. Rey-Lafon, C. Sourisseau, *Mol. Phys.* **1989**,
39 *67* 665.
40
41 [37] J. Li, D. Dunstan, X. Lou, A. Planes, L. Mañosa, M. Barrio, J.-L. Tamarit, P. Lloveras, *J. Mater.*
42 *Chem. A* **2020**, *8* 20354.
43
44 [38] E. Brück, H. Yibole, L. Zhang, *Philos. Trans. A Math. Phys. Eng. Sci.* **2016**, *374* 20150303.
45
46 [39] L. Mañosa, A. Planes, *Appl. Phys. Lett.* **2020**, *116* 050501.
47
48 [40] A. Aznar, P. Negrier, A. Planes, L. Mañosa, E. Stern-Taulats, X. Moya, M. Barrio, J.-L. Tamarit,
49 P. Lloveras, *Appl. Mater. Today* **2021**, *23* 101023.
50
51
52
53
54
55
56
57
58
59
60
61
62
63
64
65




Click here to access/download
Supporting Information
Supplementary Material.pdf






Click here to access/download
Production Data
Figure1.pdf



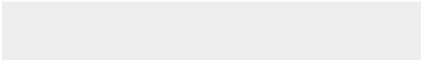




Click here to access/download
Production Data
Figure2.pdf



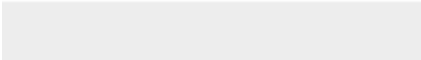



Click here to access/download
Production Data
Figure3.pdf






Click here to access/download
Production Data
Figure4.pdf





Click here to access/download
Production Data
Figure5.pdf






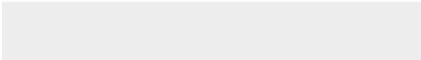

Click here to access/download

Production Data
Figure6.pdf





Click here to access/download
Production Data
Figure7.pdf





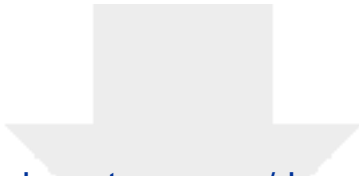
Click here to access/download
Production Data
MSP-template.bib





Click here to access/download
Production Data
MSP.bst

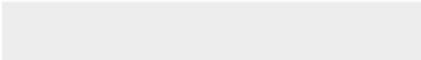




Click here to access/download

Production Data

07a81d23-0aa0-4d42-bfd4-d1726431d4ee





Click here to access/download
Production Data
Revised Manuscript.tex





Click here to access/download
Production Data
VCH-logo.png





Click here to access/download
Production Data
WileyMSP-template.cls

